Journal of Computational Physics 229 (2010) 6156–6179

Contents lists available at ScienceDirect

Journal of Computational Physics

journal homepage: www.elsevier.com/locate/jcp

A local high-order doubly asymptotic open boundary for diffusion in a semi-infinite layer

C. Birk [a,*], Ch. Song [b]

[a] Institut für Statik und Dynamik der Tragwerke, Fakultät Bauingenieurwesen, Technische Universität Dresden, 01062 Dresden, Germany
[b] School of Civil and Environmental Engineering, University of New South Wales, Sydney, NSW 2052, Australia

ARTICLE INFO

Article history:
Received 10 November 2009
Received in revised form 28 April 2010
Accepted 28 April 2010
Available online 6 May 2010

Keywords:
High-order open boundary
Doubly asymptotic
Semi-infinite layer
Diffusion
Heat equation
Continued-fraction expansion
Fractional derivative

ABSTRACT

A high-order open boundary for transient diffusion in a semi-infinite homogeneous layer is developed. The method of separation of variables is used to derive a relationship between the modal function and the flux at the near field/far field boundary in the Fourier domain. The resulting equation in terms of the modal impedance coefficient is solved by expanding the latter into a doubly asymptotic series of continued fractions. As a result, the open boundary condition in the Fourier domain is represented by a system of algebraic equations in terms of $\sqrt{i\omega}$. This corresponds to a system of fractional differential equations of degree $\alpha = 0.5$ in the time-domain. This temporally global formulation is transformed into a local description by introducing internal variables. The resulting local high-order open boundary condition is highly accurate, as is demonstrated by a number of heat transfer examples. A significant gain in accuracy is obtained in comparison with existing singly-asymptotic formulations at no additional computational cost.

1. Introduction

The computational modelling of transient diffusion problems is required in a number of engineering and physics applications, including heat transfer, mass transport, option pricing or diffuse optical imaging. Special attention has to be paid if the diffusion process occurs in a very large domain, which can be assumed as unbounded. Most of the existing literature on modelling diffusion in unbounded domains can be classified as either a boundary integral approach [1–7] or application of a domain discretization method such as the finite-element method [8–11] or finite difference method [12–14]. Since in the former case the computational cost can become prohibitively expensive with increasing problem size, recent research efforts have been devoted to the development of fast methods [15,16].

If the finite-element method or finite difference method is used to model diffusion, the computational domain is truncated by an artificial boundary. Here, appropriate boundary conditions are required to accurately model the effect of diffusion into the unbounded medium. Extensive literature on such boundary conditions exists, which is reflected in several review articles such as [17–19]. Ref. [17] is closely related to this paper, since it is devoted to the Schrödinger equation, a basic equation in quantum mechanics, which is (formally) similar to the diffusion equation. Recent developments on boundary conditions for Schrödinger-type equations can be found in Refs. [20,14,21,22], for example. Refs. [18,19] are more general, but also address diffusion in unbounded domains.

Boundary conditions that behave identically to the unbounded domain truncated by the artificial boundary are referred to as 'exact boundary conditions'. Formulations which yield approximations of the original solution are known as 'absorbing

* Corresponding author. Tel.: +49 351 4633 5325; fax: +49 351 4633 7086.
E-mail addresses: Carolin.Birk@tu-dresden.de (C. Birk), c.song@unsw.edu.au (Ch. Song).

0021-9991/$ - see front matter © 2010 Elsevier Inc. All rights reserved.
doi:10.1016/j.jcp.2010.04.046

boundary conditions' (ABC's). In general, exact boundary conditions are highly accurate but global with respect to time and space and thus computationally expensive. Exact boundary conditions for the diffusion equation have been derived and tested for some special situations, such as for the heat equation in one and two-dimensions [8,12], and for the one-dimensional heat equation on a semi-infinite line, in a region bounded by a circular cylinder and in a region bounded by a sphere [9,13]. As mentioned above, local absorbing boundary conditions are desirable for time-domain calculations. Examples of ABC's for diffusion and their applications can be found in [10,11,23,24]

Alternative approaches for diffusion problems include the thin-layer method [25] or the scaled boundary finite-element method [26]. Both techniques are semi-analytical and based on a discretization of the governing equations in the direction of layering or in the circumferential directions, respectively. The solution in the radial direction is expressed analytically. Both the thin-layer method and the scaled boundary finite-element method have originally been formulated in the Fourier domain. In Ref. [26], a direct time-domain formulation for transient diffusion is obtained by expanding the stiffness matrix calculated with the scaled boundary finite-element method into a series of continued fractions. The resulting system of algebraic equations in terms of $\sqrt{i\omega}$ is interpreted as a system of fractional differential equations in the time-domain. Here, the singly-asymptotic continued-fraction expansion developed in Ref. [27] by Bazyar and Song for wave propagation problems is used. This asymptotic expansion is highly accurate for high frequencies, but converges very slowly in the low-frequency range. As has been demonstrated in Ref. [28], it cannot be used for (layered) systems with a cut-off frequency. Moreover, instability problems can occur for problems with a large number of degrees of freedom [26].

An advance towards mimicking wave propagation in an unbounded domain over the entire frequency range is the introduction of doubly asymptotic boundaries [29–33]. This formulation is spatially global as the dynamic stiffness is exact not only at the high-frequency limit but also at statics. To the authors knowledge, the highest order reported is three [33].

An alternative approach is to approximate the square root $\sqrt{1+z}$ by a rational function with complex coefficients, as proposed in Ref. [34]. This idea has been applied to absorbing boundaries for acoustic scattering in Ref. [35]. For high values of z, the Padé expansion proposed in Ref. [34] tends to a complex constant value. This conflicts with the asymptotic behaviour of the diffusion problem considered herein. Moreover, the use of complex coefficients is undesirable in a time-domain analysis.

Recently, Prempramote et al. [28] extended the work in Ref. [27] by constructing high-order doubly asymptotic open boundaries of arbitrary order for the scalar wave equation. The corresponding continued-fraction expansion of the dynamic stiffness converges rapidly to the exact solution in the frequency domain as its order increases. Scalar wave propagation in waveguides is modelled by a system of first-order differential equations in the time-domain with real coefficients, which can easily be coupled to finite-element models. Evanescent waves and late-time responses are simulated accurately, no stability problems are observed.

In this paper, a highly accurate high-order open boundary for diffusion is developed by extending the previous work of the authors on wave propagation in unbounded domains [28] and on the numerical solution of fractional differential equations [36]. Diffusion in a homogeneous semi-infinite layer is addressed. This is a special case of stratified semi-infinite media which are of technological importance, for example, in biomedical engineering [37] or heat diffusion [25]. Although only the semi-infinite layer is considered in this paper, it should be noted that the proposed technique can be readily applied to other important problems which can be solved using the method of separation of variables. These include the circular cavity embedded in a full plane and the sphere embedded in full space. The open boundaries derived for these cases can be used directly for the solution of practical problems by introducing straight or circular artificial boundaries. Further work on modelling diffusion problems with more complicated geometries and inhomogeneities is in progress.

The outline of this paper is as follows. In Section 2, the governing partial differential equations of the two-dimensional diffusion problem are transformed into a set of ordinary differential equations using the method of separation of variables. A modal impedance coefficient is defined, which relates the Fourier transform of the modal flux to the Fourier transform of the unknown modal function at the vertical boundary. An algebraic equation for this impedance coefficient as a function of ω, the dual variable of the time t, is derived.

In Section 3, a high-order open boundary is obtained by expanding the modal impedance coefficient into a doubly asymptotic series of continued fractions. For wave propagation [28], the continued-fraction solution can be expressed as a series of linear equations in the frequency domain, which corresponds to a system of first-order differential equations in the time-domain. For diffusion, however, a system of linear equations formulated in terms of $\sqrt{i\omega}$ is obtained, which corresponds to a system of fractional differential equations in the time-domain. This is demonstrated in Section 4. The fractional operator is global, which is disadvantageous from a computational point of view, as the evaluation of a convolution integral is required.

In Section 5, a local high-order open boundary condition for diffusion is obtained transforming the above system of fractional differential equations into a system of first-order differential equations in the time-domain. In Section 6, a corresponding efficient time-discretization scheme is developed. The proposed method is used to study several heat conduction problems in Section 7.

2. Modal decomposition of diffusion equation in semi-infinite layer

Heat conduction in a semi-infinite two-dimensional layered medium of constant thickness h as shown in Fig. 1(a) is considered in this paper. In general, the domain is split into a rectangular near field region Ω_N and a semi-infinite far

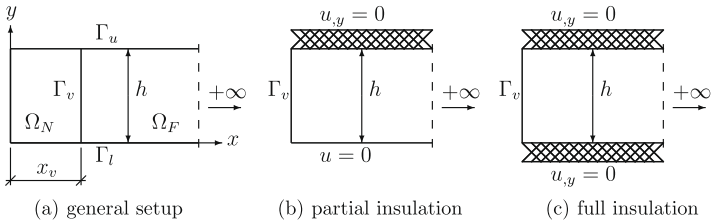

Fig. 1. Semi-infinite layer with constant depth h.

field region Ω_F. The two domains are linked by the artificial boundary Γ_v at $x = x_v$. Typically, we are interested in the numerical solution of the diffusion problem in the bounded region Ω_N. This solution can be computed using the well-established finite-element method provided that a suitable boundary condition at the artificial boundary Γ_v is available. This boundary condition should be formulated such that diffusion in the semi-infinite domain Ω_F, which is eliminated from the computation, is accurately represented. The aim of this paper is to formulate such an open boundary condition which is suitable for the analysis of transient diffusion problems. Therefore, we focus on the semi-infinite region Ω_F in the following. The method of separation of variables can be applied to obtain a series of one-dimensional differential equations to describe diffusion in Ω_F.

2.1. Semi-infinite layer with constant depth

The homogeneous heat equation is expressed as:

$$\nabla^2 u = \frac{\mu}{\kappa}\dot{u}, \tag{1}$$

where $u = u(x,y,t)$ denotes the temperature field, κ is the thermal conductivity and $\mu = \rho c$ is the product of the mass density ρ and the specific heat c of the material. The flux $q(x,y,t)$ is defined as

$$q(x,y,t) = -\kappa u_{,x}(x,y,t). \tag{2}$$

It is assumed that a distributed flux q_v is applied to the vertical (artificial) boundary Γ_v.

$$q_v = q(x = x_v, y, t) = -\kappa u_{,x}(x = x_v, y, t). \tag{3}$$

Here and in the following, the subscript 'v' indicates the position x_v. The boundary conditions prescribed at the parallel upper boundary Γ_u and lower boundary Γ_l are satisfied by eigenfunctions using the method of separation of variables. Two different situations are considered in the following. The first case, depicted in Fig. 1(b), is referred to as the 'partially insulated' situation. Here, zero temperature is prescribed at the lower boundary Γ_l, whereas the upper boundary Γ_u is assumed to be insulated, corresponding to zero normal flux. In the second case, referred to as 'fully insulated' (Fig. 1(c)), the normal flux is zero at both the upper and lower parallel boundaries.

The temperature field $u = u(x,y,t)$ is written as the product of two functions $\tilde{u} = \tilde{u}(x,t)$ and $Y = Y(y)$:

$$u = \tilde{u}Y. \tag{4}$$

Substituting Eq. (4) in Eq. (1) yields:

$$\tilde{u}_{,xx}Y + \tilde{u}Y_{,yy} = \frac{\mu}{\kappa}\dot{\tilde{u}}Y. \tag{5}$$

Dividing by $\tilde{u}Y$, Eq. (5) is transformed in two independent differential equations: an ordinary differential equation with respect to the vertical coordinate y (Eq. (6)), and a partial differential equation with respect to x and t (Eq. (7)):

$$-\frac{Y_{,yy}}{Y} = k, \tag{6}$$

$$\frac{\tilde{u}_{,xx}}{\tilde{u}} - \frac{\mu}{\kappa}\frac{\dot{\tilde{u}}}{\tilde{u}} = k. \tag{7}$$

For convenience, the constant k is chosen as $k = \frac{\lambda^2}{h^2}$. The ordinary differential Eq. (6) is rewritten as

$$0 = Y_{,yy} + \frac{\lambda^2}{h^2}Y. \tag{8}$$

Its solution is expressed as

$$Y = C_1 \cos\left(\lambda\frac{y}{h}\right) + C_2 \sin\left(\lambda\frac{y}{h}\right). \tag{9}$$

The integration constants C_1 and C_2 are determined by the boundary conditions at Γ_u and Γ_l. The resulting eigenvalues λ_j and eigenfunctions $Y_j = Y_j(y)$ are summarized in Eqs. (10) and (11) for the partially and fully insulated situation, respectively.

$$\left.\begin{array}{l}\cos\lambda = 0,\\ \lambda_j = (2j+1)\frac{\pi}{2}, \quad j = 0,1,\ldots\\ Y_j = \sin\left(\lambda_j \frac{y}{h}\right)\end{array}\right\} \quad \begin{array}{l}\Gamma_l : u = 0,\\ \Gamma_u : u_{,y} = 0\end{array} \tag{10}$$

$$\left.\begin{array}{l}\sin\lambda = 0,\\ \lambda_j = j\pi, \quad j = 0,1,\ldots\\ Y_j = \cos\left(\lambda_j \frac{y}{h}\right)\end{array}\right\} \quad \begin{array}{l}\Gamma_l : u_{,y} = 0,\\ \Gamma_u : u_{,y} = 0\end{array} \tag{11}$$

Note that the first mode of the fully insulated layer ($\lambda_0 = 0$) corresponds to a constant eigenfunction, $Y_0 = 1$. The solution of the remaining partial differential Eq. (7) with respect to x and t for one eigenvalue λ_j is addressed next:

$$\tilde{u}_{j,xx} - \left(\frac{\lambda_j}{h}\right)^2 \tilde{u}_j = \frac{\mu}{\kappa}\dot{\tilde{u}}_j. \tag{12}$$

2.2. Analytical solution

Eq. (12) is transformed into the Fourier domain:

$$\widetilde{U}_{j,xx} - \left(\frac{\lambda_j}{h}\right)^2 \widetilde{U}_j = i\omega\frac{\mu}{\kappa}\widetilde{U}_j. \tag{13}$$

The symbol $\widetilde{U}_j = \widetilde{U}_j(x,\omega)$ is the Fourier transform of the modal temperature $\tilde{u}_j$ defined as

$$\widetilde{U}_j(\omega) = \mathcal{F}\{\tilde{u}_j(t)\} = \int_{-\infty}^{+\infty} \tilde{u}_j(t)\mathrm{e}^{-i\omega t}\, dt, \tag{14}$$

with the inverse operation:

$$\tilde{u}_j(t) = \mathcal{F}^{-1}\left\{\widetilde{U}_j(\omega)\right\} = \frac{1}{2\pi}\int_{-\infty}^{+\infty} \widetilde{U}_j(\omega)\mathrm{e}^{i\omega t}\, d\omega. \tag{15}$$

The symbol ω denotes the dual variable of time t. Using the dimensionless parameter a with:

$$a = \omega\frac{\mu}{\kappa}h^2, \tag{16}$$

the solution of Eq. (13) leading to a finite modal temperature at $x \to \infty$ is expressed as

$$\widetilde{U}_j = C\cdot \mathrm{e}^{-\sqrt{\lambda_j^2 + ia}\frac{x}{h}}. \tag{17}$$

For the semi-infinite layer extending to the right-hand side, the Fourier transform $Q(x,y,\omega)$:

$$Q(x,y,\omega) = \mathcal{F}\{q(x,y,t)\}, \tag{18}$$

of the flux $q(x,y,t)$ as defined in Eq. (2) is expressed after modal decomposition of the temperature field as

$$Q(x,y,\omega) = -\kappa\sum_{j=0}^{\infty}\left(\widetilde{U}_j(x,\omega)\right)_{,x} Y_j(y). \tag{19}$$

A modal flux-temperature relationship, which is independent of y, is obtained by making use of the orthogonality of the eigenfunctions Y_j. Multiplying Eq. (19) by Y_j and integrating over the depth of the layer we obtain for one mode j:

$$\int_{y=0}^{h} Q(x,y,\omega)Y_j(y)\, dy = -\frac{\kappa}{2}h\left(\widetilde{U}_j(x,\omega)\right)_{,x}. \tag{20}$$

The symbol $\widetilde{R}_j = \widetilde{R}_j(x,\omega)$ is introduced to denote the modal flux at a vertical boundary:

$$\widetilde{R}_j(x,\omega) = \frac{2}{\kappa}\int_{y=0}^{h} Q(x,y,\omega)Y_j(y)\, dy. \tag{21}$$

Eq. (22) follows from Eqs. (20) and (21) as

$$\widetilde{R}_j = -h\widetilde{U}_{j,x}, \tag{22}$$

with:

$$\widetilde{U}_{j,x} = -\sqrt{\lambda_j^2 + ia}\frac{1}{h}C\cdot\mathrm{e}^{-\sqrt{\lambda_j^2+ia}\frac{x}{h}} = -\sqrt{\lambda_j^2+ia}\frac{1}{h}\widetilde{U}_j. \tag{23}$$

On the other hand, at the vertical boundary Γ_v the Fourier transform of the modal flux $\widetilde{R}_j(x_v)$ is related to the Fourier transform of the modal temperature $\widetilde{U}_j(x_v)$ through:

$$\widetilde{R}_j(x_v,a) = S(a)\widetilde{U}_j(x_v,a). \tag{24}$$

The flux-temperature relationship is characterized by the coefficient $S(a)$, which is a function of the dimensionless parameter a and thus of ω, the dual variable of time t. It is referred to as *impedance coefficient* in the following. Evaluating Eq. (23) at $x = x_v$ and equating Eqs. (22) and (24), the modal impedance coefficient of the semi-infinite layer is obtained as

$$S(a) = \sqrt{\lambda_j^2 + ia}. \tag{25}$$

Eqs. (24) and (25) form the analytical solution in the Fourier domain. To obtain a reference solution to validate numerical results in the time-domain, the response to a unit-step modal flux $\tilde{r}_{jS}(x_v,t) = H(t)$:

$$H(t) = \begin{cases} 0 & \text{for} \quad t < 0, \\ 1.0 & \text{for} \quad t \geqslant 0, \end{cases} \tag{26}$$

applied at $x = x_v$, $t = 0$ is evaluated. The Fourier transform of the unit-step function is $\widetilde{R}_{jS}(x_v) = \frac{1}{i\omega}$. The Fourier transform $\widetilde{U}_{jS}(x_v)$ of the modal temperature due to the above unit-step modal flux $\tilde{r}_{jS}(x_v)$ follows from Eqs. (24) and (25):

$$\widetilde{U}_{jS}(x_v) = \frac{1}{ia\sqrt{\lambda_j^2 + ia}} \cdot \frac{\mu h^2}{\kappa}. \tag{27}$$

The unit-step response $\tilde{u}_{jS}(x_v)$ in the time-domain is obtained by applying the inverse Fourier transformation (15) to Eq. (27). For $\widetilde{U}_{jS}(x_v)$ given in Eq. (27), the Fourier integral can be evaluated in closed form, see for example [38,39]. We obtain:

$$\tilde{u}_{jS}(x_v,t) = \frac{1}{\lambda_j}\operatorname{erf}\left(\lambda_j\sqrt{\bar{t}}\right)H(\bar{t}), \tag{28}$$

with the dimensionless time:

$$\bar{t} = \frac{\kappa}{\mu h^2}t. \tag{29}$$

Note that Eq. (28) is valid for all modes of the partially insulated layer, but for the modes $j \geqslant 1$ of the fully insulated layer only. For $\lambda_0 = 0$, the impedance coefficient $S(a)$ in Eq. (25) simplifies to:

$$S^{\lambda_0=0}(a) = \sqrt{ia}. \tag{30}$$

The corresponding unit-step response in the time-domain is

$$\tilde{u}_{0S}(x_v,t) = \mathcal{F}^{-1}\left\{\frac{1}{i\omega\sqrt{ia}}\right\} = \frac{2}{\sqrt{\pi}}\sqrt{\bar{t}}H(\bar{t}). \tag{31}$$

Analogously, the unit-impulse response $\tilde{u}_{jI}(x_v,t)$, that is the modal temperature due to a unit-impulse modal flux $\tilde{r}_{jI}(x_v,t) = \delta(t)$, is obtained applying the inverse Fourier transformation to the inverse of the impedance coefficient $S(\omega)$:

$$\tilde{u}_{jI}(x_v,t) = \mathcal{F}^{-1}\left\{\frac{1}{\sqrt{\lambda_j^2 + ia}}\right\} = \frac{\kappa}{\mu h^2}\frac{1}{\Gamma(1/2)}\frac{1}{\sqrt{\bar{t}}}\mathrm{e}^{-\lambda_j^2\bar{t}}H(\bar{t}). \tag{32}$$

Again, Eq. (32) is valid for $\lambda_j \neq 0$ only. The unit-impulse response for $\lambda_0 = 0$ is derived analogously to Eq. (32):

$$\tilde{u}_{0I}(x_v,t) = \sqrt{\frac{\kappa}{\mu h^2}}\mathcal{F}^{-1}\left\{\frac{1}{\sqrt{i\omega}}\right\} = \frac{1}{\sqrt{\pi\bar{t}}}H(\bar{t}). \tag{33}$$

The temperature response due to an arbitrary prescribed modal flux $\tilde{r}_j(x_v,t)$ can finally be expressed as a convolution integral:

$$\tilde{u}_j(x_v,t) = \int_0^t \tilde{u}_{jI}(x_v,t-\tau)\tilde{r}_j(x_v,\tau)\,d\tau = \int_0^t \tilde{u}_{jS}(x_v,t-\tau)\dot{\tilde{r}}_j(x_v,\tau)\,d\tau. \tag{34}$$

Note that the unit-impulse response $\tilde{u}_{jI}(x_v,t)$ is unbounded for $t \to 0$. Alternatively, the Fourier transform of a given modal flux $\tilde{r}_j(x_v,t)$ can be computed and the problem can be solved in the Fourier domain. The modal temperature in the time-domain is then obtained by applying the inverse Fourier transformation to the Fourier domain result.

The numerical evaluation of the convolution integral in Eq. (34) can be computationally expensive for longer observation times and is not desired in a general time-domain analysis. In order to derive a local formulation, the problem is recast in terms of the modal impedance coefficient $S(a)$ in the following.

2.3. Formulation in terms of modal impedance coefficient

An equation for the modal impedance coefficient is obtained rewriting Eq. (25) as

$$S^2 = \lambda_j^2 + ia. \tag{35}$$

Using the following substitution:

$$ia = A^2, \tag{36}$$

it can be cast in a form which is similar to the equation of the modal dynamic stiffness coefficient of a semi-infinite layer derived in the context of wave propagation in Ref. [28]:

$$S^2 = \lambda_j^2 + A^2. \tag{37}$$

Eq. (37) can be solved by expanding $S(A)$ into a doubly asymptotic series of continued fractions in terms of A. Following the procedure described in Ref. [28], the coefficients of the continued-fraction expansion are obtained as functions of the eigenvalue λ_j. Thus, a different continued-fraction representation is constructed for each mode j. This is avoided normalizing both the impedance coefficient S and the auxiliary parameter A with respect to the eigenvalue λ_j:

$$\overline{S} = \frac{S}{\lambda_j}, \quad \overline{A} = \frac{A}{\lambda_j}, \tag{38}$$

Using Eqs. (38), (37) is rewritten as

$$\overline{S}^2 = 1 + \overline{A}^2. \tag{39}$$

3. Doubly asymptotic expansion of normalized modal impedance coefficient in terms of $\overline{A}$

The continued-fraction solution of Eq. (39) is demonstrated in the following. The procedure is analogous to the derivation presented in Ref. [28], but differs in that only one and the same continued-fraction expansion is obtained for all modes of the semi-infinite layer. In a first step, an asymptotic expansion of the normalized impedance coefficient valid for high values $|\overline{A}| \to \infty$ is constructed analogous to Ref. [27].

3.1. Asymptotic expansion for $|\overline{A}| \to \infty$

For high values $|\overline{A}| \to \infty$, the normalized impedance coefficient $\overline{S}$ tends to $\overline{A}$. This can easily be verified considering Eq. (39). For arbitrary values $\overline{A}$, the normalized impedance coefficient is expressed as

$$\overline{S} = \overline{A} - \left(Y^{(1)}(\overline{A})\right)^{-1}. \tag{40}$$

In Eq. (40) the term $(Y^{(1)}(\overline{A}))^{-1}$ represents the residual of the asymptotic expansion, i.e. the difference between the normalized impedance coefficient and its value for $|\overline{A}| \to \infty$. The residual tends to zero for $|\overline{A}| \to \infty$. For convenience, it is expressed as the inverse of a yet unknown function $Y^{(1)}(\overline{A})$ of $\overline{A}$. The superscript (1) indicates the first step of a recursive procedure, as will become evident further in the derivation. Substituting Eq. (40) in Eq. (39) results in:

$$-1 - 2\overline{A}\left(Y^{(1)}(\overline{A})\right)^{-1} + \left(Y^{(1)}(\overline{A})\right)^{-2} = 0. \tag{41}$$

Eq. (41) can be written as the $i = 1$ case of:

$$1 - 2b^{(i)}\overline{A}Y^{(i)}(\overline{A}) - \left(Y^{(i)}(\overline{A})\right)^2 = 0, \tag{42}$$

with

$$b^{(1)} = 1. \tag{43}$$

Analogous to Eq. (40), the unknown function $Y^{(i)}(\overline{A})$ is decomposed as

$$Y^{(i)}(\overline{A}) = \overline{A}C^{(i)} - \left(Y^{(i+1)}(\overline{A})\right)^{-1}. \tag{44}$$

Here, we assume that $Y^{(i)}(\overline{A})$ tends to a linear function of $\overline{A}$ for $|\overline{A}| \to \infty$. The slope $C^{(i)}$ of this linear function is yet unknown. Substituting Eq. (44) in Eq. (42) yields:

$$-\overline{A}^2\left((C^{(i)})^2 + 2b^{(i)}C^{(i)}\right) + 1 + 2\overline{A}\left(C^{(i)} + b^{(i)}\right)\left(Y^{(i+1)}(\overline{A})\right)^{-1} - \left(Y^{i+1}(\overline{A})\right)^{-2} = 0. \tag{45}$$

This is an equation for the coefficient $C^{(i)}$ and for the yet unknown residual $(Y^{(i+1)}(\overline{A}))^{-1}$. Individual equations are obtained by setting terms corresponding to different powers of $\overline{A}$ to zero in descending order. Setting the first term of Eq. (45) (i.e. $\overline{A}^2$) to zero yields an equation for $C^{(i)}$:

$$C^{(i)} = -2b^{(i)}, \tag{46}$$

For $i = 1$ we obtain $C^{(1)} = -2$. Setting the remainder of Eq. (45) to zero using Eq. (46) leads to an equation for $Y^{(i+1)}(\overline{A})$:

$$1 + 2\overline{A}b^{(i)}Y^{(i+1)}(\overline{A}) - \left(Y^{(i+1)}(\overline{A})\right)^2 = 0. \tag{47}$$

The recursive formula:

$$b^{(i+1)} = -b^{(i)}, \tag{48}$$

is introduced to update the coefficient b. Using Eq. (48), Eq. (47) can be written as

$$1 - 2\overline{A}b^{(i+1)}Y^{(i+1)}(\overline{A}) - \left(Y^{(i+1)}(\overline{A})\right)^2 = 0. \tag{49}$$

This is the $(i+1)$ case of Eq. (42). General equations for $b^{(i)}$ and $C^{(i)}$ follow from Eqs. (43), (48) and (46) as

$$b^{(i)} = (-1)^{i+1}, \quad i = 1, 2, \ldots, M_H, \tag{50}$$

$$C^{(i)} = (-1)^i 2, \quad i = 1, 2, \ldots, M_H. \tag{51}$$

After $i = M_H$ steps, the normalized impedance coefficient is expressed as

$$\overline{S} = \overline{A} - \cfrac{1}{C^{(1)}\overline{A} - \cfrac{1}{C^{(2)} - \cdots \cfrac{1}{C^{(M_H)} - \left(Y^{(M_H+1)}(\overline{A})\right)^{-1}}}}. \tag{52}$$

For a given order M_H, the coefficients $C^{(i)}$, $(i = 1 \ldots M_H)$ of this continued-fraction expansion can be calculated using Eq. (51). The remaining residual $(Y^{(M_H+1)}(\overline{A}))^{-1}$ is yet unknown. In order to find a solution which is valid over the whole range of $|\overline{A}|$, the remaining residual term $(Y^{(M_H+1)}(\overline{A}))^{-1}$ is determined such that the final doubly asymptotic expansion of $\overline{S}(\overline{A})$ is exact for $|\overline{A}| \to 0$.

3.2. Asymptotic expansion for $|\overline{A}| \to 0$

The inverse $Y^{(M_H+1)}(\overline{A})$ of the residual term corresponding to a continued-fraction expansion for high values $|\overline{A}| \to \infty$ of degree M_H is denoted as

$$Y^{(M_H+1)}(\overline{A}) = Y_L(\overline{A}). \tag{53}$$

Using Eq. (53), the $i = M_H + 1$ case of Eq. (42) is written as

$$1 - 2\overline{A}b_L Y_L(\overline{A}) - \left(Y_L(\overline{A})\right)^2 = 0, \tag{54}$$

with

$$b_L = b^{(M_H+1)} = (-1)^{M_H}. \tag{55}$$

The unknown function $Y_L(\overline{A})$ is expanded as

$$Y_L(\overline{A}) = K_L^{(0)} + \overline{A}C_L^{(0)} - \overline{A}^2\left(Y_L^{(1)}(\overline{A})\right)^{-1}. \tag{56}$$

This expansion is designed such that $Y_L(\overline{A})$ approaches the constant $K_L^{(0)}$ for $|\overline{A}| \to 0$, whereas the yet undetermined linear term $\overline{A}C_L^{(0)}$ and the residual $\overline{A}^2(Y_L^{(1)}(\overline{A}))^{-1}$ vanish. Substituting Eq. (56) in Eq. (54) yields:

$$\begin{aligned} &1 - \left(K_L^{(0)}\right)^2 - \overline{A}\left(2b_L K_L^{(0)} + 2K_L^{(0)}C_L^{(0)}\right) \\ &\quad + \overline{A}^2\left(-2b_L C_L^{(0)} - \left(C_L^{(0)}\right)^2 + 2\left(K_L^{(0)} + \overline{A}\left(C_L^{(0)} + b_L\right)\right)\left(Y_L^{(1)}(\overline{A})\right)^{-1} - \overline{A}^2\left(Y_L^{(1)}(\overline{A})\right)^{-2}\right) = 0. \end{aligned} \tag{57}$$

Equations for $K_L^{(0)}$, $C_L^{(0)}$ and $(Y_L^{(1)}(\overline{A}))^{-1}$ are found by setting terms corresponding to different powers of $\overline{A}$ to zero in ascending order. The constant term (i.e. $\overline{A}^0$) yields:

$$1 - (K_L^{(0)})^2 = 0. \tag{58}$$

Eq. (58) has two possible solutions. The one leading to the correct normalized impedance for $\overline{A} = 0$, $\overline{S}(\overline{A} = 0) = 1$, should be chosen. This is

$$K_L^{(0)} = (-1)^{M_H+1}. \tag{59}$$

Note that the sign of $K_L^{(0)}$ depends on the order of continued-fraction expansion M_H for high values of $|\overline{A}|$. The linear term in Eq. (57) leads to an equation for $C_L^{(0)}$:

$$C_L^{(0)} = -b_L = (-1)^{M_H+1}. \tag{60}$$

The remaining term in Eq. (57) yields an equation for the unknown function $Y_L^{(1)}(\overline{A})$:

$$\overline{A}^2 - 2\left(K_L^{(0)} + \overline{A}\left(C_L^{(0)} + b_L\right)\right)Y_L^{(1)}(\overline{A}) + \left(2b_L C_L^{(0)} + \left(C_L^{(0)}\right)^2\right)\left(Y_L^{(1)}(\overline{A})\right)^2 = 0. \tag{61}$$

Using Eqs. (59) and (60), (61) can be written as the $i = 1$ case of:

$$\overline{A}^2 - 2b_L^{(i)}Y_L^{(i)}(\overline{A}) - \left(Y_L^{(i)}(\overline{A})\right)^2 = 0, \tag{62}$$

with

$$b_L^{(1)} = -b_L = (-1)^{M_H+1}. \tag{63}$$

Analogous to Eq. (56) the unknown function $Y_L^{(i)}(\overline{A})$ is decomposed as

$$Y_L^{(i)}(\overline{A}) = K_L^{(i)} - \overline{A}^2\left(Y_L^{(i+1)}(\overline{A})\right)^{-1}. \tag{64}$$

Note that the linear term is omitted in Eq. (64) as its solution is equal to zero, which can easily be verified. Substituting Eq. (64) into Eq. (62) leads to:

$$-\left(2b_L^{(i)}K_L^{(i)} + \left(K_L^{(i)}\right)^2\right) + \overline{A}^2\left(1 + 2\left(b_L^{(i)} + K_L^{(i)}\right)\left(Y_L^{(i+1)}(\overline{A})\right)^{-1} - \overline{A}^2\left(Y_L^{(i+1)}(\overline{A})\right)^{-2}\right) = 0. \tag{65}$$

In the recursive procedure, general expressions for the coefficients $K_L^{(i)}$ and for the unknown function $Y_L^{(i+1)}(\overline{A})$ are determined setting the terms corresponding to different powers of $\overline{A}$ equal to zero in ascending order. Setting the constant term equal to zero yields for $K_L^{(i)}$:

$$K_L^{(i)} = -2b_L^{(i)}. \tag{66}$$

Setting the remaining term to zero and using Eq. (66) leads to:

$$\overline{A}^2 + 2b_L^{(i)}Y_L^{(i+1)}(\overline{A}) - \left(Y_L^{(i+1)}(\overline{A})\right)^2 = 0. \tag{67}$$

Eq. (67) is the case $(i + 1)$ of Eq. (62) with:

$$b_L^{(i+1)} = -b_L^{(i)}. \tag{68}$$

Using Eq. (63), the constants $b_L^{(i)}$ and $K_L^{(i)}$ can be explicitely expressed as

$$b_L^{(i)} = (-1)^{M_H+i}, \quad i = 1, 2, \ldots, M_L, \tag{69}$$

$$K_L^{(i)} = 2(-1)^{M_H+i+1}, \quad i = 1, 2, \ldots, M_L. \tag{70}$$

The recursive procedure is terminated with the assumption $(Y_L^{(M_L+1)}(\overline{A}))^{-1} = 0$. The doubly asymptotic continued-fraction solution is constructed by combining the asymptotic expansion for $|\overline{A}| \to \infty$ with the solution for $|\overline{A}| \to 0$. For example, the order $M_H = M_L = 2$ doubly asymptotic continued-fraction solution is obtained as

$$\overline{S}(\overline{A}) = \overline{A} - \cfrac{1}{C^{(1)}\overline{A} - \cfrac{1}{C^{(2)}\overline{A} - \cfrac{1}{K_L^{(0)} + C_L^{(0)}\overline{A} - \cfrac{\overline{A}^2}{K_L^{(1)} - \cfrac{\overline{A}^2}{K_L^{(2)}}}}}}, \tag{71}$$

$$\overline{S}(\overline{A}) = \overline{A} - \cfrac{1}{-2\overline{A} - \cfrac{1}{2\overline{A} - \cfrac{1}{-1 - \overline{A} - \cfrac{\overline{A}^2}{2 - \frac{\overline{A}^2}{-2}}}}}. \tag{72}$$

It should be noted that the proposed continued-fraction expansion is equivalent to a rational function of numerator degree $M_H + M_L + 2$ and of denominator degree $M_H + M_L + 1$. This rational function can be expressed as the sum of a linear term and a series of partial fractions in terms of $\overline{A}$, i.e. in terms of $\sqrt{i\omega}$. In the context of wave propagation, Wolf [40,41] proposed to interpret partial fractions in terms of $i\omega$ as simple physical spring-damper models to represent the unbounded soil. This

idea can be extended to partial fractions in terms of $\sqrt{i\omega}$ by replacing the viscous damping element by a fractional damper of degree 0.5. This requires, however, the calculation of the poles of the denominator polynomial of the rational function, which can be a numerically difficult task. The idea presented in Refs. [40,41] cannot be extended to the matrix case.

In the following, a time-domain model for diffusion in a semi-infinite layer is obtained by transforming the continued-fraction solution (71) into a system of linear equations in terms of $\sqrt{i\omega}$. This is done by introducing internal variables. One advantage of the proposed method is that the calculation of poles is avoided. Moreover, it can be extended to the multi-dimensional case straightforwardly.

4. Implementation in the time-domain

In order to derive a time-domain equivalent of the doubly asymptotic continued-fraction expansion of the normalized impedance coefficient, the equations derived above are re-assembled, starting with Eqs. (24), (38) and (40):

$$\widetilde{R}_j(x_v) = S\widetilde{U}_j(x_v) = \lambda_j\overline{S}\widetilde{U}_j(x_v) = \left(\lambda_j\overline{A} - \lambda_j\left(Y^{(1)}(\overline{A})\right)^{-1}\right)\widetilde{U}_j(x_v). \tag{73}$$

Using $\overline{A} = A/\lambda_j$ and intoducing an internal variable $\widetilde{U}_j^{(1)}$, a first linear Eq. (74) in terms of A is obtained:

$$\widetilde{R}_j(x_v) = A\widetilde{U}_j(x_v) - \lambda_j\widetilde{U}_j^{(1)}, \tag{74}$$

with

$$\widetilde{U}_j(x_v) = Y^{(1)}(\overline{A})\widetilde{U}_j^{(1)}. \tag{75}$$

Using Eq. (44), Eq. (75) can be written as

$$\widetilde{U}_j(x_v) = \left(\overline{A}C^{(1)} - \left(Y^{(2)}(\overline{A})\right)^{-1}\right)\widetilde{U}_j^{(1)}. \tag{76}$$

A second linear Eq. (77) in terms of A is obtained introducing a second internal variable $\widetilde{U}_j^{(2)}$:

$$\lambda_j\widetilde{U}_j(x_v) = AC^{(1)}\widetilde{U}_j^{(1)} - \lambda_j\widetilde{U}_j^{(2)}. \tag{77}$$

This process is continued until a total of M_H internal variables have been introduced to represent the high-asymptotic part of the continued-fraction expansion. The (M_H+1)-th linear equation in terms of A can be written as

$$\lambda_j\widetilde{U}_j^{(M_H-1)} = AC^{(M_H)}\widetilde{U}_j^{(M_H)} - \lambda_j\widetilde{U}_j^{(M_H+1)}. \tag{78}$$

The internal variable $\widetilde{U}_j^{(M_H+1)}$ is defined as

$$\widetilde{U}_j^{(M_H)} = Y^{(M_H+1)}(\overline{A})\widetilde{U}_j^{(M_H+1)} = Y_L(\overline{A})\widetilde{U}_j^{(M_H+1)}, \tag{79}$$

with the residual $Y^{(M_H+1)}$ given in Eq. (53). Using Eq. (56), Eq. (79) can be written as

$$\widetilde{U}_j^{(M_H)} = \left(K_L^{(0)} + \overline{A}C_L^{(0)} - \overline{A}^2\left(Y_L^{(1)}(\overline{A})\right)^{-1}\right)\widetilde{U}_j^{(M_H+1)}. \tag{80}$$

The (M_H+2)-th linear Eq. (81) in terms of A follows by introducing the internal variable $\widetilde{U}_{jL}^{(1)}$ as defined in Eq. (82).

$$\lambda_j\widetilde{U}_j^{(M_H)} = \left(\lambda_jK_L^{(0)} + AC_L^{(0)}\right)\widetilde{U}_j^{(M_H+1)} - A\widetilde{U}_{jL}^{(1)}. \tag{81}$$

$$\overline{A}\left(Y_L^{(1)}(\overline{A})\right)^{-1}\widetilde{U}_j^{(M_H+1)} = \widetilde{U}_{jL}^{(1)}. \tag{82}$$

Using Eq. (64), Eq. (82) can be reformulated as

$$A\widetilde{U}_j^{(M_H+1)} = \lambda_jK_L^{(1)}\widetilde{U}_{jL}^{(1)} - A\widetilde{U}_{jL}^{(2)}, \tag{83}$$

with

$$A\widetilde{U}_{jL}^{(1)} = \lambda_jY_L^{(2)}(\overline{A})\widetilde{U}_{jL}^{(2)}. \tag{84}$$

This procedure is continued until M_L internal variables $\widetilde{U}_{jL}^{(i)}$, $(i=1,\ldots,M_L)$ have been introduced to represent the low-asymptotic part of the continued-fraction expansion. The process terminates with the assumption $Y_L^{(M_L+1)} = 0$. The final, (M_H+M_L+2)-th linear Eq. (85) in terms of A is

$$A\widetilde{U}_{jL}^{(M_L-1)} = \lambda_jK_L^{(M_L)}\widetilde{U}_{jL}^{(M_L)}. \tag{85}$$

The linear Eqs. (74), (77), (78), (81), (83), (84) and (85) can be summarized in matrix form:

$$\left(\lambda_j[K]+A[C]\right)\{Z\}=\{F\}, \tag{86}$$

with

$$\{Z\}=\left[\widetilde{U}_j(x_v)\ \widetilde{U}_j^{(1)}\ \cdots\ \widetilde{U}_j^{(M_H)}\ \widetilde{U}_j^{(M_H+1)}\ \widetilde{U}_{jL}^{(1)}\ \cdots\ \widetilde{U}_{jL}^{(M_L)}\right]^T, \tag{87}$$

$$\{F\}=\left[\widetilde{R}_j(x_v)\ 0\ \cdots\ 0\ 0\ 0\ \cdots\ 0\right]^T, \tag{88}$$

$$[K]=\begin{bmatrix} 0 & -1 & & & & & & & \\ -1 & 0 & \ddots & & & & & & \\ & \ddots & \ddots & -1 & & & & & \\ & & -1 & 0 & -1 & & & & \\ & & & -1 & K_L^{(0)} & 0 & & & \\ & & & & 0 & K_L^{(1)} & \ddots & & \\ & & & & & \ddots & \ddots & 0 & \\ & & & & & & 0 & K_L^{(M_L)} \end{bmatrix}, \tag{89}$$

$$[C]=\begin{bmatrix} 1 & 0 & & & & & & & \\ 0 & C^{(1)} & \ddots & & & & & & \\ & \ddots & \ddots & 0 & & & & & \\ & & 0 & C^{(M_H)} & 0 & & & & \\ & & & 0 & C_L^{(0)} & -1 & & & \\ & & & & -1 & 0 & \ddots & & \\ & & & & & \ddots & \ddots & -1 & \\ & & & & & & -1 & 0 \end{bmatrix}. \tag{90}$$

Using Eqs. (51), (59), (60) and (70), the matrices $[K]$ and $[C]$ can be explicitely expressed as

$$[K]=\begin{bmatrix} 0 & -1 & & & & & & & \\ -1 & 0 & \ddots & & & & & & \\ & \ddots & \ddots & -1 & & & & & \\ & & -1 & 0 & -1 & & & & \\ & & & -1 & (-1)^{M_H+1} & 0 & & & \\ & & & & 0 & 2(-1)^{M_H+2} & \ddots & & \\ & & & & & \ddots & \ddots & 0 & \\ & & & & & & 0 & 2(-1)^{M_H+M_L+1} \end{bmatrix}, \tag{91}$$

$$[C]=\begin{bmatrix} 1 & 0 & & & & & & & \\ 0 & -2 & 0 & & & & & & \\ & 0 & 2 & \ddots & & & & & \\ & & \ddots & \ddots & 0 & & & & \\ & & & 0 & 2(-1)^{M_H} & 0 & & & \\ & & & & 0 & (-1)^{M_H+1} & -1 & & \\ & & & & & -1 & 0 & \ddots & \\ & & & & & & \ddots & \ddots & -1 \\ & & & & & & & -1 & 0 \end{bmatrix}, \tag{92}$$

Eq. (86) is the flux-temperature relationship for one mode λ_j formulated in terms of A. Note that the matrices $[K]$ and $[C]$ do not depend on the eigenvalue λ_j. Recall that A is an auxiliary parameter which has been introduced to facilitate the continued-fraction expansion of the impedance coefficient. A formulation in terms of ω, the dual variable of the time t, is obtained using Eq. (36) to substitute A by $\sqrt{i\alpha}$ in Eq. (86), and using Eq. (16):

$$\left(\lambda_j[K]+\sqrt{i\omega}\sqrt{\frac{\mu}{\kappa}}h[C]\right)\{Z\}=\{F\}. \tag{93}$$

The mathematical theory of fractional calculus enables the interpretation of the term $\sqrt{i\omega}$ in the time-domain. Interest in the concept of differentiation and integration to non-integer order dates back to the 19th century and has led to a variety of approaches since then. The most frequently encountered definition of a fractional derivative of arbitrary order is the Riemann–Liouville derivative [42] defined in Eq. (94):

$$D_t^{\alpha} z(t) = \frac{1}{\Gamma(m-\alpha)} \frac{d^m}{dt^m} \int_0^t \frac{z(\tau)}{(t-\tau)^{\alpha+1-m}} d\tau, \quad m-1 < \alpha \leqslant m. \tag{94}$$

Here, m is an integer number and the symbol Γ represents the Gamma function. Tables of fractional derivatives of frequently used functions are given in Ref. [42]. Application of the Fourier transform to the Riemann–Liouville fractional derivative yields:

$$\mathcal{F}\{D_t^{\alpha} z(t)\} = (i\omega)^{\alpha} Z(\omega) - \sum_{j=0}^{m-1} (i\omega)^j D_t^{\alpha-1-j} z(t)|_{t=0}, \quad m-1 < \alpha \leqslant m, \tag{95}$$

with the Fourier transform $Z(\omega)$ of the function $z(t)$. A proof of Eq. (95) is given in the textbook [43]. The initial values of fractional derivatives occurring in Eq. (95) are set equal to zero in most cases reported in the literature. This corresponds to the assumption of $z(t)$ being equal to zero for $t \leqslant 0$. Applying the inverse Fourier transform to Eq. (93), using Eq. (95) and assuming:

$$\{z(t)\} = 0 \quad \text{for } t \leqslant 0, \tag{96}$$

leads to

$$\lambda_j [K]\{z(t)\} + \sqrt{\frac{\mu}{\kappa}} h [C] D_t^{\frac{1}{2}} \{z(t)\} = \{f(t)\}. \tag{97}$$

Eq. (97) represents the modal flux-temperature relationship of the semi-infinite layer in the time-domain. The vector $\{z(t)\}$ contains the unknown, time-dependent modal temperature $\tilde{u}_j(x_v, t)$ at the near field/far field interface and the corresponding time-dependent internal variables $\tilde{u}_j^{(1)}(t), \ldots, \tilde{u}_j^{(M_H+1)}(t)$, $\tilde{u}_{jL}^{(1)}(t), \ldots, \tilde{u}_{jL}^{(M_L)}(t)$. The right-hand side vector $\{f(t)\}$ contains the time-dependent modal flux $\tilde{r}_j(x_v, t)$ at $x = x_v$.

Eq. (97) can be non-dimensionalized introducing the normalized unknowns $\{\bar{z}\}$:

$$\{\bar{z}\} = \lambda_j \{z\}, \tag{98}$$

and formulating the problem with respect to $\lambda_j^2 \bar{t}$, where $\bar{t}$ is the dimensionless time given in Eq. (29). We obtain:

$$[K]\{\bar{z}\} + [C] D^{\frac{1}{2}}_{(\lambda_j^2 \bar{t})} \{\bar{z}\} = \{f\}. \tag{99}$$

The equivalence of Eqs. (97) and (99) is easily proven evaluating the fractional derivative with respect to $\lambda_j^2 \bar{t}$ using Eq. (98):

$$D^{\frac{1}{2}}_{(\lambda_j^2 \bar{t})} \{\bar{z}\} = \frac{1}{\Gamma(\frac{1}{2})} \frac{d}{d(\lambda_j^2 \bar{t})} \int_0^{\lambda_j^2 \bar{t}} \frac{\lambda_j \{z\}}{\left(\lambda_j^2 \bar{t} - \bar{\tau}\right)^{\frac{1}{2}}} d\bar{\tau}. \tag{100}$$

Using

$$d(\lambda_j^2 \bar{t}) = \frac{\kappa}{\mu} \frac{\lambda_j^2}{h^2} dt, \quad \bar{\tau} = \tau \frac{\kappa}{\mu} \frac{\lambda_j^2}{h^2}, \quad d\bar{\tau} = \frac{\kappa}{\mu} \frac{\lambda_j^2}{h^2} d\tau, \tag{101}$$

we obtain:

$$D^{\frac{1}{2}}_{(\lambda_j^2 \bar{t})} \{\bar{z}\} = \frac{1}{\Gamma(\frac{1}{2})} \frac{\mu}{\kappa} \frac{h^2}{\lambda_j^2} \frac{d}{dt} \int_0^{\tau = \bar{t} \frac{\mu h^2}{\kappa} = t} \frac{\lambda_j \{z\}}{\sqrt{\frac{\kappa}{\mu}} \frac{\lambda_j}{h} (t-\tau)^{\frac{1}{2}}} \frac{\kappa}{\mu} \frac{\lambda_j^2}{h^2} d\tau \tag{102}$$

$$= \frac{1}{\Gamma(\frac{1}{2})} \sqrt{\frac{\mu}{\kappa}} h \frac{d}{dt} \int_0^t \frac{\{z\}}{(t-\tau)^{\frac{1}{2}}} d\tau = \sqrt{\frac{\mu}{\kappa}} h D_t^{\frac{1}{2}} \{z(t)\}. \tag{103}$$

The proposed procedure should be used for the numerical analysis of all modes with $\lambda_j \neq 0$. For $\lambda_0 = 0$ (i.e. the first mode of the fully insulated layer) the modal impedance relationship (24) simplifies to:

$$\widetilde{R}_0(x_v) = \sqrt{ia}\widetilde{U}_0(x_v) = \sqrt{\frac{\mu h^2}{\kappa}} \sqrt{i\omega} \widetilde{U}_0(x_v). \tag{104}$$

This corresponds directly to the scalar fractional differential Eq. (105):

$$D_t^{\frac{1}{2}}\tilde{u}_0(x_v,t) = \sqrt{\frac{\kappa}{\mu h^2}}\tilde{r}_0(x_v,t). \tag{105}$$

Thus, it is not necessary to expand the modal impedance coefficient $S^{\lambda_0=0}$ into a series of continued fractions. The fractional differential Eqs. (97), (99) and (105) can be transformed into systems of ordinary differential equations as described in the next section.

5. Temporally local formulation

Using Eq. (97) or (99), the modal temperature $\tilde{u}_j(x_v,t)$ due to an arbitrary transient flux $q_v(t)$ can be calculated directly in the time-domain. A direct time-domain model for the semi-infinite layer is obtained by modal superposition of Eq. (97) or (99) for several modes λ_j. The resulting formulation can be coupled to a finite element model for diffusion in a bounded domain via the flux $q(x = x_v,t)$.

Several methods for the numerical solution of fractional differential equations by means of direct integration exist, for example [44–47]. These algorithms are based on a discretization of the convolution integral associated with fractional differentiation. They lead to storage and evaluation of the complete history in each time step, which is disadvantageous from a computational point of view. Therefore, alternative schemes that attempt to replace the global fractional operator by a local operator have been proposed [48,36]. These schemes are based on expressing the fractional convolution kernel as an improper integral with exponential integrand which is then evaluated numerically using Gauss–Laguerre integration. They are closely related to the method of Jiang and Greengard [49], who express the convolution kernel of the exact non-reflecting boundary condition for the Schrödinger equation using the same integral representation and approximate the latter using Gauss–Legendre quadrature on dyadic intervals. Jiang and Greengard also presented a detailed error analysis and established a rule to determine the number of quadrature points necessary to achieve a given accuracy. The number of quadrature points used in Ref. [49] is, however, considerably larger than the number of internal variables introduced in Refs. [48,36].

The method proposed in Ref. [48] has been used successfully by some authors [48,50], but critisized by others [51,52] for its slow convergence. Recently, Diethelm [53] presented a modification of the algorithms presented in Refs. [48,36], which leads to increased accuracy. Diethelm's method is applicable to fractional derivatives of arbitrary degree. In the following, it is applied to Eq. (97) and thus adapted to the case $\alpha = \frac{1}{2}$, which considerably simplifies the notation.

The fractional derivative (94) is rewritten using Leibniz's rule and integrating by parts as

$$D_t^{\frac{1}{2}}\{z(t)\} = \frac{1}{\Gamma\left(\frac{1}{2}\right)}\int_0^t \frac{\{\dot{z}(\tau)\}}{(t-\tau)^{\frac{1}{2}}}\,d\tau. \tag{106}$$

In order to replace the fractionally decaying memory by such of exponentially decaying type, the following relationships for the Gamma function of positive real argument v are used:

$$\Gamma(v) = \int_0^\infty \mathrm{e}^{-x}x^{v-1}\,dx, \quad v > 0, \quad v \in \mathbb{R}, \tag{107}$$

$$\frac{1}{\Gamma(1-v)} = \frac{\Gamma(v)}{\pi}\sin\pi v. \tag{108}$$

Substituting Eqs. (107) and (108) in Eq. (106) yields for $v = \frac{1}{2}$:

$$D_t^{\frac{1}{2}}\{z(t)\} = \frac{1}{\pi}\int_0^t\int_0^\infty \mathrm{e}^{-x}\left(\frac{x}{t-\tau}\right)^{\frac{1}{2}}\frac{1}{x}\{\dot{z}(\tau)\}\,dx\,d\tau. \tag{109}$$

After a final substitution of

$$x = (t-\tau)p^2 \;\rightarrow\; dx = 2(t-\tau)p\,dp, \tag{110}$$

in Eq. (109), the fractional derivative of order $\alpha = \frac{1}{2}$ is written as

$$D_t^{\frac{1}{2}}\{z(t)\} = \frac{2}{\pi}\int_0^t\int_0^\infty \mathrm{e}^{-(t-\tau)p^2}\{\dot{z}(\tau)\}\,dp\,d\tau. \tag{111}$$

The decisive idea is to replace the integral with respect to time in Eq. (111) by a new variable $\{\phi(p,t)\}$:

$$D_t^{\frac{1}{2}}\{z(t)\} = \frac{2}{\pi}\int_0^\infty \{\phi(p,t)\}\,dp, \tag{112}$$

$$\{\phi(p,t)\} = \int_0^t \mathrm{e}^{-(t-\tau)p^2}\{\dot{z}(\tau)\}\,d\tau. \tag{113}$$

The integral Eq. (113) is equivalent to the first-order differential Eq. (114). This can easily be verified by differentiation of Eq. (113) using Leibniz's rule.

$$\left\{\dot{\phi}(p,t)\right\} + p^2\{\phi(p,t)\} = \{\dot{z}(t)\}. \tag{114}$$

The remaining integral in Eq. (112) is evaluated numerically using Gaussian quadrature. This is facilitated using the following substitutions:

$$q = \frac{1-p}{1+p}, \quad p = \frac{1-q}{1+q}, \tag{115}$$

$$\{\bar{\phi}(q,t)\} = 2(1+q)^{-2}\{\phi(p,t)\}, \tag{116}$$

$$\int_0^{\infty} \{\phi(p,t)\}\, dp = \int_{-1}^{+1} \{\bar{\phi}(q,t)\}\, dq. \tag{117}$$

In the following we concentrate on the numerical solution of the normalized fractional differential Eq. (99), for conciseness. The derived algorithm can straightforwardly be used for the solution of Eq. (97), replacing the matrices $[K]$ and $[C]$ by their counterparts $\lambda_j[K]$ and $\frac{\mu}{\kappa}h[C]$, respectively. The system of Eqs. (118)–(120) for the solution of (99) follows:

$$[K]\{\bar{z}\} + \frac{4}{\pi}[C] \times \sum_{i=1}^{L} W_{iL}(1+Z_{iL})^{-2}\{\phi_i\} = \{f\}, \tag{118}$$

$$\{\dot{\phi}_1\} + (Y_{1L})^2\{\phi_1\} = \{\dot{\bar{z}}\}, \tag{119}$$

$$\vdots$$

$$\{\dot{\phi}_L\} + (Y_{LL})^2\{\phi_L\} = \{\dot{\bar{z}}\}. \tag{120}$$

In Eq. (118) the symbols W_{iL} and Z_{iL} denote the weights and abscissas of Gaussian integration with respect to the weight function $W(q) = 1$ over the integral $(-1,1)$ for L integration points, and

$$Y_{iL} = \frac{1-Z_{iL}}{1+Z_{iL}}. \tag{121}$$

Eqs. (118)–(120) can be summarized in matrix form:

$$[B]\{\dot{x}\} = [A]\{x\} + \{f^*\}, \tag{122}$$

with

$$\{x\}^T = \left\{\{\bar{z}\}^T\ \{\phi_1\}^T\ \cdots\ \{\phi_L\}^T\right\}, \quad \{f^*\}^T = \left\{\{f\}^T\ \{0\}^T\ \cdots\ \{0\}^T\right\}. \tag{123}$$

The coefficient matrix $[B]$ in Eq. (122) is of order $(M_H + M_L + 2) \times (L+1)$. If a standard time-stepping scheme is used to solve the system of ordinary differential equations (122), the introduction of internal variables yields to an undesirable increase in computational effort. This can be avoided using an efficient method presented by Adhikari and Wagner [54] for the numerical solution of a state-space representation of the equations of motion of exponentially damped systems. This approach, which is based on the elimination of the internal variables, is adapted to the solution of Eq. (122) in the following section.

6. Efficient solution in the time-domain

The trapezoidal rule is used to approximate the state vector $\{x\}$:

$$\{x(\tau)\} = \{x\}_k\left(1 - \frac{\tau}{\Delta t}\right) + \{x\}_{k+1}\frac{\tau}{\Delta t}, \quad 0 \leqslant \tau \leqslant \Delta t, \tag{124}$$

within one time step of length Δt. Using the linear approximation (124) and integrating Eqs. (119), (120) within the front time interval yields:

$$\{\phi_i\}_{k+1} - \{\phi_i\}_k + \frac{\Delta t}{2}(Y_{iL})^2\left(\{\phi_i\}_k + \{\phi_i\}_{k+1}\right) = \{\bar{z}\}_{k+1} - \{\bar{z}\}_k. \tag{125}$$

Eq. (125) can be used to eliminate the internal variables $\{\phi_i\}_{k+1}$:

$$\{\phi_i\}_{k+1} = \frac{1}{1+\frac{\Delta t}{2}(Y_{iL})^2}\left(\{\bar{z}\}_{k+1} - \{\bar{z}\}_k\right) + \frac{1-\frac{\Delta t}{2}(Y_{iL})^2}{1+\frac{\Delta t}{2}(Y_{iL})^2}\{\phi_i\}_k, \quad i = 1,\ldots,L. \tag{126}$$

Substituting Eq. (126) into Eq. (118) and using the linear approximation (124) yields the following algorithm for the calculation of the variables $\{\bar{z}\}_{k+1}$ at the end of the time step Δt by means of the values $\{\bar{z}\}_k$ and the internal variables $\{\phi_i\}_k$ at the beginning of the time step:

$$([K] + v[C])\{\bar{z}\}_{k+1} = v[C]\{\bar{z}\}_k - \sum_{i=1}^{L} \mu_i [C]\{\phi_i\}_k + \{f\}_{k+1}, \tag{127}$$

with

$$v = \frac{4}{\pi} \sum_{i=1}^{L} W_{iL} (1 + Z_{iL})^{-2} \frac{1}{1 + \frac{\Delta t}{2}(Y_{iL})^2},$$

$$\mu_i = \frac{4}{\pi} W_{iL} (1 + Z_{iL})^{-2} \left(\frac{1 - \frac{\Delta t}{2}(Y_{iL})^2}{1 + \frac{\Delta t}{2}(Y_{iL})^2} \right).$$

The coefficient matrix ($[K] + v[C]$) in Eq. (127) is of order ($M_H + M_L + 2$), and thus of the same order as the original fractional differential Eq. (97). Eqs. (127) and (126) allow for an efficient and accurate solution of the system of first-order differential Eqs. (118)–(120), despite a large number of internal variables.

The total computational cost of the proposed approach is directly proportional to the numbers of modes considered. For each mode, the local high-order open boundary condition is expressed as a system of linear equations of order ($M_H + M_L + 2$) with tridiagonal coefficient matrices. The influence of the number of quadrature points on the numerical cost is negligible. Thus, the numerical effort increases linearly with the orders of doubly asymptotic expansion M_H and M_L.

7. Numerical examples

7.1. Single mode of the semi-infinite layer

A single mode λ_j of the semi-infinite layer is considered. The normalized modal impedance coefficient $\bar{S}$ is shown in Figs. 2 and 3. In Fig. 2, $\bar{S}$ is plotted as a function of the auxiliary parameter A^2 for values A^2 ranging from $-3\lambda_j^2$ to zero. This

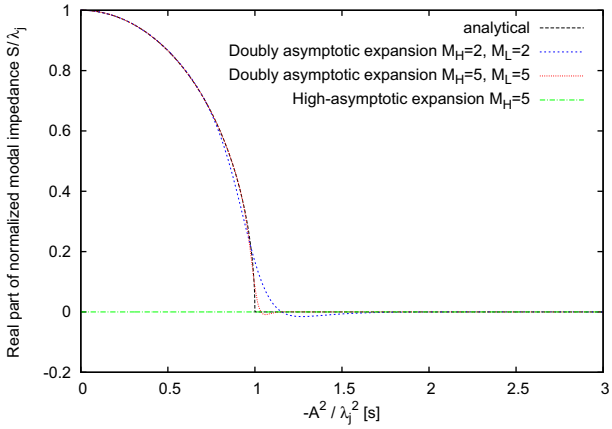

(a) Real part

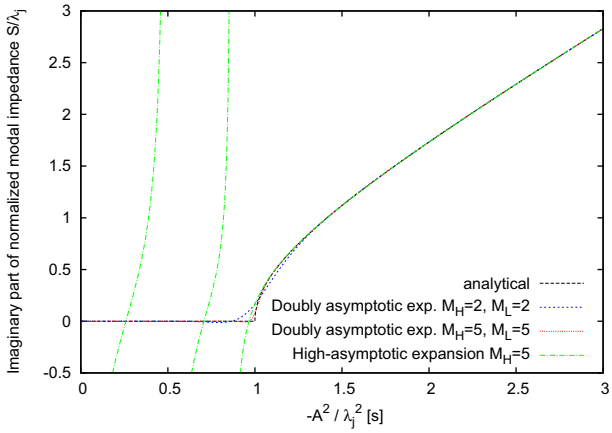

(b) Imaginary part

Fig. 2. Normalized modal impedance coefficient $\bar{S}$ of semi-infinite layer as a function of the auxiliary parameter $A^2 = ia$.

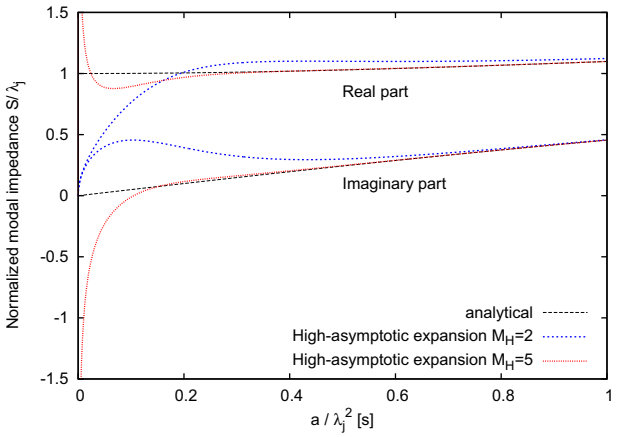

(a) High-asymptotic expansion

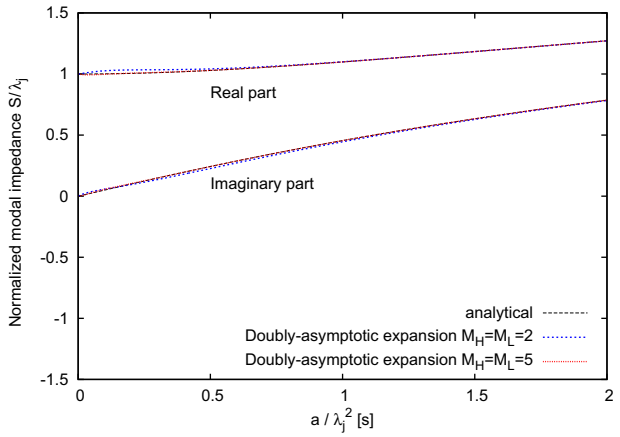

(b) Doubly asymptotic

Fig. 3. Normalized modal impedance coefficient $\overline{S}$ of semi-infinite layer as a function of $a = \omega\frac{\mu}{\kappa}h^2$.

corresponds to a dimensionless frequency a ranging from $a = 0$ to $a = 3i \cdot \lambda_j^2$. Although this parameter range is not relevant from a physical point of view, it is addressed here because it provides insight into the method of expanding $\overline{S}$ into a series of continued fractions.

The curves shown in Fig. 2 are well-known in the context of wave propagation (see for example Figs. 3–5 in Ref. [28]). The point $-A^2/\lambda_j^2 = 1$ corresponds to the cut-off frequency in a wave propagation analysis. It can be seen that the doubly asymptotic expansion of degree $M_H = M_L = 2$ agrees very well with the corresponding analytical solution. Slight deviations occur in the vicinity of $-A^2/\lambda_j^2 = 1$. This can be improved by increasing the degree of expansion, as can be seen for $M_H = M_L = 5$. The corresponding high-asymptotic expansion is also shown for $M_H = 5$. Above the characteristic point $-A^2/\lambda_j^2 = 1.0$ a very good agreement, comparable to that of the doubly asymptotic expansion of degree $M_H = M_L = 2$, is achieved using the high-asymptotic expansion. However, for values below $-A^2/\lambda_j^2 = 1.0$ the imaginary part of the high-asymptotic expansion diverges. Its real part is always zero, as is expected. Fig. 2 illustrates that the high-frequency asymptotic expansion of Ref. [27] fails when wave propagation in a semi-infinite layer is modelled.

The performance of the high-asymptotic and the doubly asymptotic expansion for diffusion in a semi-infinite layer is addressed in Fig. 3(a) and (b), respectively. Here, $\overline{S}$ is plotted as a function of the dimensionless parameter a, the dual variable of the dimensionless time $\bar{t}$. From a physical point of view, only real positive values of a are meaningful. For such real positive values of a, the modal impedance coefficient $S(a)$ given in Eq. (25) is always complex, the cut-off phenomenon known from wave propagation does not exist for diffusion. Nevertheless, it is obvious from Fig. 3(a) that the accuracy of the high-asymptotic expansion proposed in Ref. [27] and used for the time-domain analysis of a three-dimensional diffusion problem in Ref. [26] is poor for small values of a. This is explained as follows. The high-frequency-asymptotic expansion of degree M_H of the normalized impedance coefficient can be formulated in terms of ia as

$$\bar{S}(a) = \sqrt{i\bar{a}} - \cfrac{1}{-2\sqrt{i\bar{a}} - \cfrac{1}{2\sqrt{i\bar{a}} - \cfrac{1}{\cdots - \cfrac{1}{(-1)^{M_H} 2\sqrt{i\bar{a}}}}}}, \tag{128}$$

with

$$\bar{a} = \frac{a}{\lambda_j^2}.$$

For a approaching zero, the impedance coefficient $\bar{S}(a)$ given in Eq. (128) approaches zero, if an even degree M_H is chosen. It tends to infinity, if M_H is odd. This is illustrated in Fig. 3(a) for $M_H = 2$ and $M_H = 5$, respectively. In either case the high-asymptotic expansion of the impedance coefficient fails for small values of a and in particular for $a = 0$. The poor approximation of $\bar{S}(a)$ for $a \to 0$ affects the accuracy of the late-time response, and in particular the steady-state response of the semi-infinite layer.

Contrary to the high-asymptotic expansion of the modal impedance coefficient, the doubly asymptotic continued-fraction expansion proposed in this paper is exact for $a = 0$. This is guaranteed by the choice of the coefficient $K_L^{(0)}$ according to Eq. (59), as described in Section 3.2. Moreover, the doubly asymptotic boundary is designed such that it converges to the exact impedance coefficient throughout the complete a-range, if the orders of expansion M_H and M_L are increased. Fig. 3(b) shows that a very good agreement between the analytical and the approximate impedance coefficient is achieved already using expansion orders as low as $M_H = 2$ and $M_L = 2$. For $a < 1.0$, small differences between the approximate and the exact curve can be seen. The agreement between the analytical impedance coefficient and the doubly asymptotic expansion of degree $M_H = M_L = 5$ is excellent.

The convergence of the proposed doubly asymptotic expansion with increasing degree M_H and M_L is further studied in Fig. 4. Fig. 4(a) and (b) show the absolute error in real and imaginary part of the normalized impedance coefficient $\bar{S}$, respectively, obtained using continued-fraction solutions of increasing order M_H and M_L. The error is zero for $a = 0$ and for very high values of a, as is expected for a doubly asymptotic approximation. The error in the intermediate range depends on M_H and M_L. In general, the difference between exact and approximate impedance coefficient is smaller for higher values of M_H and M_L. As observed in Fig. 3(a) and (b), the biggest error occurs in the range $0 < a < 1.0$. However, the absolute error quickly decreases as the order of expansion M_H and M_L increases.

The stability of the system of fractional differential equations (97) to represent one mode of the semi-infinite layer is addressed. Here, the term 'stability' refers to a physically consistent decaying behaviour of homogeneous solutions. Fractional differential equations, like (97), however, are not characterized by simple exponential homogeneous solutions. A stability criterion for fractional differential equations with a smallest common denominator equal to two is derived in Ref. [55]. As for first-order differential equations, the solution of an associated eigenvalue problem is required in order to evaluate the stability of fractional differential equations. In case of the semi-differential Eq. (97) this eigenvalue problem is of the form:

$$([K] + v[C])\{x\} = 0. \tag{129}$$

Unstable solution parts of fractional differential equations with a smallest common denominator equal to two correspond to auxiliary eigenvalues v_j with:

$$-\frac{\pi}{4} < \arg(v_j) < \frac{\pi}{4}. \tag{130}$$

For a detailed derivation of Eq. (130) the reader is referred to Ref. [55].

The matrices $[K]$ and $[C]$ in Eq. (129) result from the continued-fraction expansion of the normalized impedance coefficient $\bar{S}$ presented in Section 3. The corresponding eigenvalues v_j have been calculated for various degrees of expansion M_H and M_L. Selected results are given in Table 1. It can be seen that for $M_H = M_L = 2$, $M_H = M_L = 5$ and $M_H = M_L = 20$ all eigenvalues v_j are located on the left-hand side of the complex plane. The corresponding fractional differential equations are thus stable. Analogous results have been obtained for other degrees of expansion. In practice, we have encountered no difficulties even for very high degrees of expansion ($M_H = M_L = 500$). This indicates that the fractional differential equation resulting from the doubly asymptotic expansion of the normalized impedance coefficient is stable, regardless of the degree of expansion.

The modal temperature response to a unit-step modal flux is computed using the proposed procedure. The normalized impedance coefficient $\bar{S}(\bar{A})$ is expanded into a doubly asymptotic series of continued fractions as described in Section 3. The degrees M_H and M_L of the two expansions for high and low values of $\bar{A}$, respectively, are chosen as $M_H = M_L = 2$. The number of internal variables involved in the transformation of the fractional differential equation to a local description is $L = 20$. The computed normalized modal temperature $\bar{u}_j(x_v, t)\lambda_j$ is compared to the analytical solution given in Eq. (28) in Fig. 5. The agreement between analytical and numerical solution is excellent.

The error introduced by the localization of the system of fractional differential Eq. (97) is addressed. Fig. 6 shows the error between the modal temperature response due to a unit-step modal flux computed using the proposed procedure and the corresponding analytical solution (28) for different numbers of quadrature points L. The degree of continued-fraction expansion is fixed, $M_H = M_L = 2$. Although the absolute error reported in the above example is generally small, big differences between the solutions obtained using $L = 5$, $L = 10$ or $L = 20$ quadrature points can be seen. In general, the maximum error

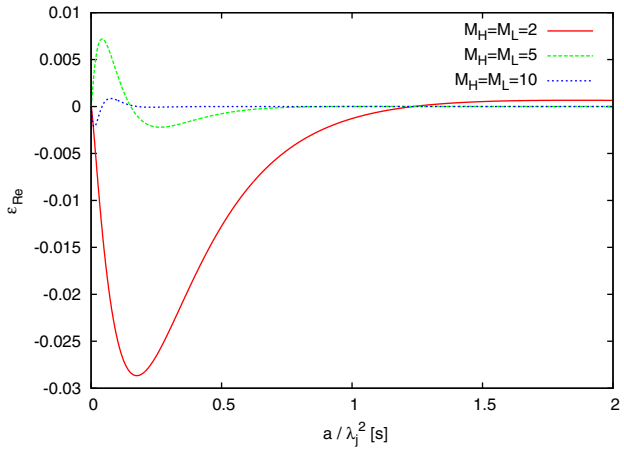

(a) $\varepsilon_{Re} = \Re\{\bar{S}_{\text{exact}}\} - \Re\{\bar{S}_{\text{continued fraction}}\}$

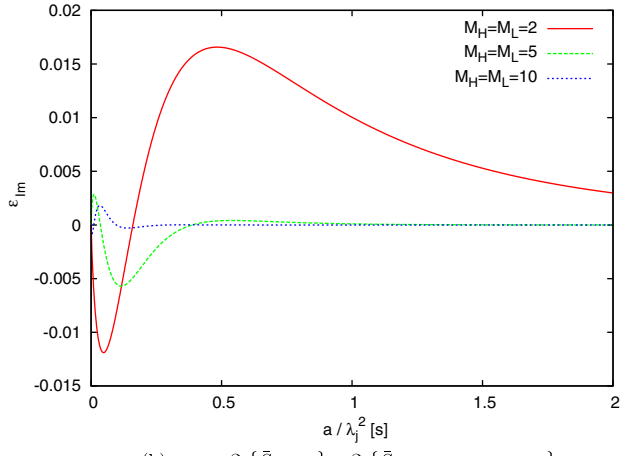

(b) $\varepsilon_{Im} = \Im\{\bar{S}_{\text{exact}}\} - \Im\{\bar{S}_{\text{continued fraction}}\}$

Fig. 4. Absolute error in normalized modal impedance coefficient $\bar{S}$ of semi-infinite layer as a function of $a = \omega\frac{\mu}{\kappa}h^2$.

Table 1
Eigenvalues v of $([K] + v[C])\{x\} = 0$ corresponding to doubly asymptotic continued-fraction expansion of modal impedance coefficient.

$M_H = 2$, $M_L = 2$		$M_H = 5$, $M_L = 5$		$M_H = 20$, $M_L = 20$	
1,2	(−0.93301270, ±0.35984344)	1,2	(−0.98296291, ±0.18380400)	1,2	(−0.99854052, ±0.06509116)
3,4	(−0.50000000, ±0.86602540)	3,4	(−0.85355339, ±0.52100538)	3,4	(−0.98787943, ±0.14680957)
5,6	(−0.06698730, ±0.99775383)	5,6	(−0.62940952, ±0.77707378)	5,6	(−0.96454670, ±0.26867033)
		7,8	(−0.37059048, ±0.92879637)	7,8	(−0.93413701, ±0.35433306)
		9,10	(−0.01703709, ±0.99985486)	9,10	(−0.88983875, ±0.45702465)
		11,12	(−0.14644661, ±0.98921858)	11,12	(−0.84085995, ±0.54114168)
				13,14	(−0.78124273, ±0.62415867)
				15,16	(−0.71712135, ±0.69700832)
				17,18	(−0.64731745, ±0.76219397)
				19,20	(−0.57453718, ±0.81848680)
				21,22	(−0.49999660, ±0.86602541)
				23,24	(−0.42547944, ±0.90496844)
				25,26	(−0.35262234, ±0.93576567)
				27,28	(−0.28305814, ±0.95910276)
				29,30	(−0.21833997, ±0.97587277)
				31,32	(−0.15991363, ±0.98713101)
				33,34	(−0.10908426, ±0.99403251)
				35,36	(−0.06698730, ±0.99775383)
				37,38	(−0.00139810, ±0.99999902)
				39,40	(−0.01253604, ±0.99992142)
				41,42	(−0.03456313, ±0.99940252)

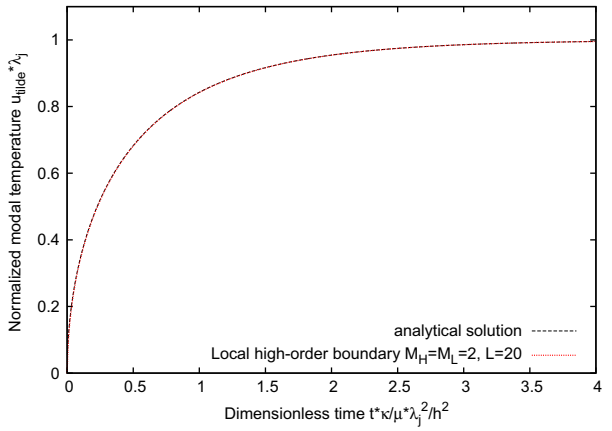

Fig. 5. Normalized modal temperature $\tilde{u}_j(t)$ at $x = x_v$ due to unit-step modal flux r_{jS} applied at $x = x_v$, $t = 0$. ($\lambda_j \neq 0$).

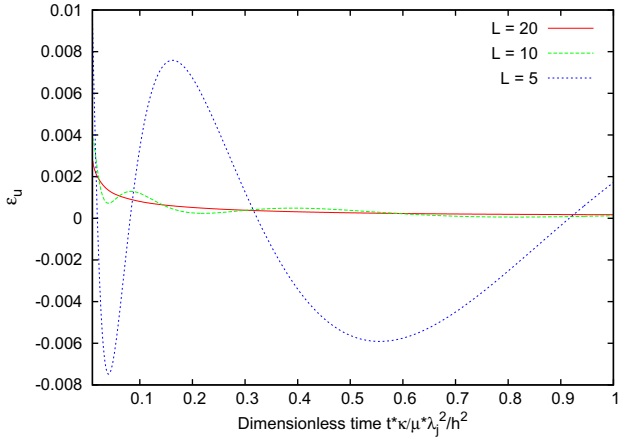

Fig. 6. Error ε_u in normalized modal temperature $\tilde{u}_j(t)$ at $x = x_v$ due to unit-step modal flux r_{jS} applied at $x = x_v$, $t = 0$. ($\lambda_j \neq 0$). $\frac{\varepsilon_u}{\lambda_j} = \tilde{u}_{j,\text{exact}} - \tilde{u}_{j,\text{numerical}}$. $M_H = M_L = 2$.

occurs for early times $\bar{t}$. The total difference between exact and numerical solution diminishes with increasing time. The numerical solution obtained using only $L = 5$ quadrature points oscillates around the exact solution. These oscillations are less pronounced for higher values of L. The order of magnitude of the maximum error obtained using $L = 20$ quadrature points is approximately 0.3% of the steady-state response. This is in agreement with the excellent result shown in Fig. 5.

The modal temperature response to a prescribed transient modal flux is also computed using the proposed procedure. The time-dependence of the modal flux is shown in Fig. 7 – a rectangular pulse of amplitude R_j and duration $\lambda_j^2 \Delta\bar{t} = \lambda_j^2 \Delta t \frac{\kappa}{\mu h^2}$. The resulting modal temperature $\tilde{u}_j(x_v, t)$ is plotted in Fig. 8. The normalized impedance coefficient $\overline{S}(\overline{A})$ is expanded into a doubly asymptotic series of continued fractions as described in Section 3. The degrees M_H and M_L of the two expansions for high and low values of $\overline{A}$, respectively, are chosen as $M_H = M_L = 2$. The number of internal variables involved in the transformation

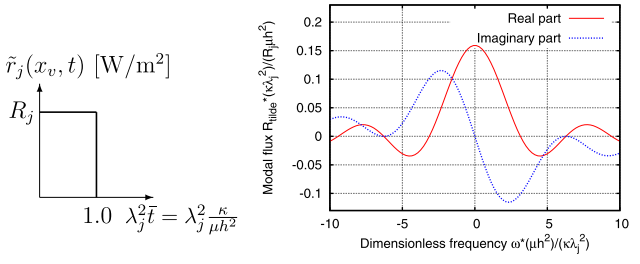

(a) Time variation (b) Fourier transform

Fig. 7. Prescribed modal flux $\tilde{r}_j(x_v, t)$.

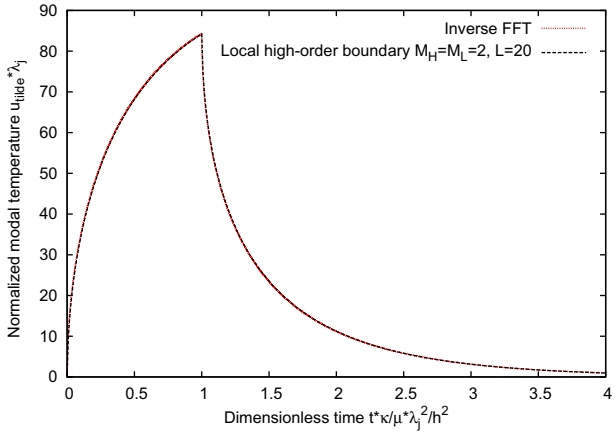

Fig. 8. Normalized modal temperature $\tilde{u}_j$ at $x = x_v$ due to prescribed modal flux (rectangular pulse $R_j = 100\frac{W}{m^2},\ \Delta\bar{t} = 1.0,\ \lambda_j \neq 0$).

of the fractional differential equation to a local description is $L = 20$. An alternative solution is obtained by solving the problem in the Fourier domain as described in Section 2. The Fourier transformation of the prescribed modal flux $\tilde{r}_j(x_v, t)$ can be evaluated in closed form. It is given in Eq. (131) and shown in Fig. 7 in a non-dimensional form:

$$\widetilde{R}_j(x_v, \omega) = \frac{1}{2\pi}\int_{-\infty}^{+\infty} r_j(x_v, t)\mathrm{e}^{-i\omega t}\,dt = \frac{R_j}{2\pi}\left(\frac{\sin\omega h}{\omega} - i\left(\frac{1-\cos\omega h}{\omega}\right)\right). \tag{131}$$

The modal temperature $\tilde{u}_j(x_v, t)$ is obtained applying the inverse Fourier transformation to $\widetilde{U}_j(x_v)$. Fig. 8 shows an extremely good agreement between the time-dependent modal temperature $\tilde{u}_j(x_v, t)$ computed using the high-order boundary and the reference solution.

7.2. Two-dimensional analysis

In a truly two-dimensional analysis, the temperature field $u(x = x_v, y, t)$ due to an arbitrary given flux $q(x = x_v, y, t)$ at $x = x_v$ is obtained by modal superposition:

$$u(x = x_v, y, t) = \sum_{j=1}^{\infty} \tilde{u}_j(x_v, t) Y_j(y). \tag{132}$$

The time-dependent modal temperature $\tilde{u}_j(x_v, t)$ is calculated directly in the time-domain using the time-stepping scheme (127). For each mode j, the right hand-side vector $\{f\}_{k+1}$ in Eq. (127) contains the corresponding value $\tilde{r}_j(x_v, k\Delta t)$ of the time-dependent modal flux $\tilde{r}_j(x_v, t)$, which is obtained evaluating Eq. (21) at $x = x_v$:

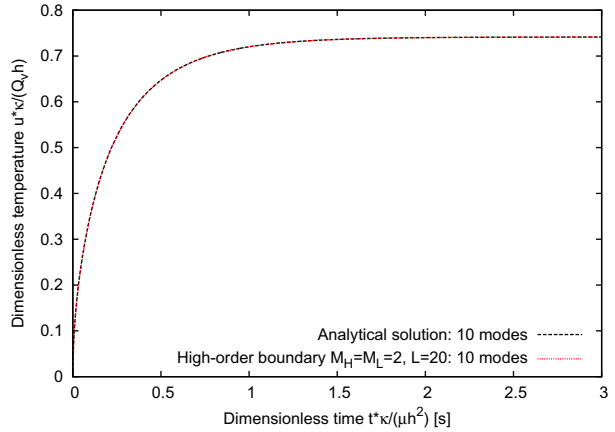

Fig. 9. Partially insulated layer (Fig. 1(b)). Dimensionless temperature $u(t)^{*}\kappa/Q_v h$ at $(x = x_v, y = h)$ due to prescribed uniform unit-step flux $q_v(y,t) = Q_v$.

$$\{f(t)\} = \left[\tilde{r}_j(x_v,t)\ 0\ \cdots\ 0\right]^T, \tag{133}$$

$$\tilde{r}_j(x_v,t) = \frac{2}{\kappa}\int_0^h q_v(y,t)Y_j(y)\,dy. \tag{134}$$

A uniform unit-step prescribed flux, $q_v(y,t) = Q_v$, acting on the partially insulated layer is considered first (Fig. 9). An analytical solution for the resulting temperature distribution at $x = x_v$ is constructed superimposing the modal unit-step response given in Eq. (28) of all modes λ_j:

$$\left.\begin{array}{l}\Gamma_u : u = 0,\\ \Gamma_l : u_{,y} = 0\end{array}\right\} \quad u(x_v,y,t) = \frac{2Q_v h}{\kappa}\sum_{j=0}^{\infty}\frac{1}{\lambda_j^2}\operatorname{erf}\left(\lambda_j\sqrt{\frac{\kappa t}{\mu h^2}}\right)\sin\left(\lambda_j\frac{y}{h}\right). \tag{135}$$

A comparison between the time-dependent temperature at the point $(x = x_v, y = h)$ computed using the presented approach with $M_H = M_L = 2$, $L = 20$ and the corresponding analytical solution is shown in Fig. 9. The results are presented in a non-dimensional form and are valid for all material parameters κ and μ and arbitrary layer thickness h. Only the first 10 modes have been taken into account. The solution using 20 modes is almost indistinguishable from the curves displayed in Fig. 9 and not shown here for clarity. As for the single mode, the agreement between the analytical solution and the proposed approach is excellent. Fig. 9 confirms the high-accuracy of the proposed high-order open boundary for diffusion and the suitability of the transformation of the system of fractional differential equations into a local formulation.

For illustration, diffusion in a semi-infinite layer which is insulated on both parallel surfaces is considered as a second example. It is assumed that the system is subject to a prescribed flux which acts over a certain part of the vertical boundary Γ_v only. A uniform distribution of flux over Δy as shown in Fig. 10 is considered. The flux is assumed to be zero over the rest of the width of the layer. That is, the vertical surface Γ_v is insulated for $\Delta y < y \leqslant h$. The problem could be of practical interest in environmental engineering, when modelling the diffusion of a pollutant of given concentration in a stream, for example. The proposed model can be used to study the influence of the height Δy on the distribution of the unknown function u over h.

An analytical reference solution is available for a prescribed unit-step flux, $q_v(t) = Q_v$:

$$\left.\begin{array}{l}\Gamma_u : u_{,y} = 0,\\ \Gamma_l : u_{,y} = 0\end{array}\right\} \quad u(x_v,y,t) = \frac{2Q_v}{\kappa}\frac{\Delta y}{h}\sqrt{\frac{\kappa}{\mu}}\sqrt{\frac{t}{\pi}} + \sum_{j=1}^{\infty}\frac{2Q_v h}{\kappa\lambda_j^2}\sin\left(\lambda_j\frac{\Delta y}{h}\right)\operatorname{erf}\left(\lambda_j\sqrt{\frac{\kappa}{\mu h^2}t}\right)\cos\left(\lambda_j\frac{y}{h}\right). \tag{136}$$

Note that the sum in Eq. (136) vanishes as Δy approaches the width of the layer h. If the fully insulated layer is subject to a uniform flux over its full width, the task of finding the resulting function u reduces to a one-dimensional problem. The analytical solution reduces to the contribution of the first mode, $\lambda_0 = 0$ in this case. Note that the latter is not bounded, but grows as a function of $\sqrt{t}$ with increasing time. If the given flux $q_v(t)$ is effective over a certain portion Δy of the width h, however, more than one mode contribute to the solution. The smaller the ratio $\frac{\Delta y}{h}$, the more modes have to be taken into account to accurately model diffusion in the fully insulated layer. This is illustrated in Fig. 11(a) and (b).

These figures show the numerically obtained temperature distribution over the width of the layer for different points in time, using a dimensionless notation. It can be seen that the temperature distribution due to the uniform prescribed flux initially follows a nearly rectangular distribution for $0 \leqslant y \leqslant \Delta y$, whereas it is almost zero for $y > \Delta y$. As regions above Δy heat up, the distribution gradually changes until a smooth limiting shape is reached. This is due to the fact that the modal response for $\lambda \neq 0$ is governed by the error-function, $\operatorname{erf}\left(\lambda_j\sqrt{\frac{\kappa}{\mu h^2}t}\right)$, see Eqs. (28) and (136), and thus bounded by 1.0.

The performance of the proposed doubly asymptotic boundary for different degrees of expansion M_H, M_L, is studied in Fig. 11(a) and (b). In Fig. 11(a) a situation where the uniform flux acts over half of the width of the layer is modelled. Here, 10 modes are sufficient to accurately model diffusion in the semi-infinite layer. The numerical solution based on a doubly asymptotic expansion of degree $M_H = M_L = 2$ agrees extremely well with the corresponding analytical solution for $\bar{t} = 0.01$, $\bar{t} = 0.1$ and $\bar{t} = 1.0$. The degree of expansion can even be reduced to $M_H = M_L = 1$ at no significant loss of accuracy.

Fig. 11(b) shows the corresponding results for a situation where the uniform flux acts over one tenth of the width of the layer. Here, 20 modes have been considered in order to accurately model diffusion in the semi-infinite layer. Again, excellent agreement between the analytical solution given in Eq. (136) and the temperature distribution at $\bar{t} = 0.01$, $\bar{t} = 0.1$ and

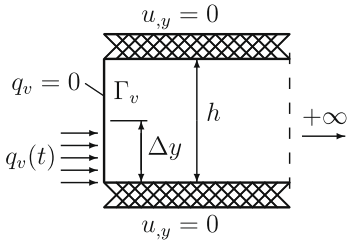

Fig. 10. Fully insulated semi-infinite layer with constant depth h, partially subject to uniform flux.

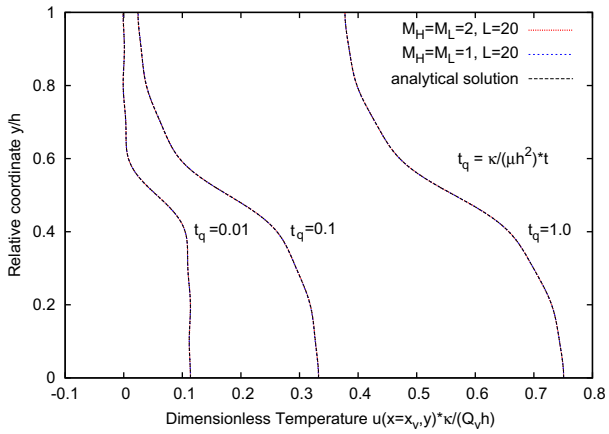

(a) $\frac{\Delta y}{h} = \frac{1}{2}$, 10 modes

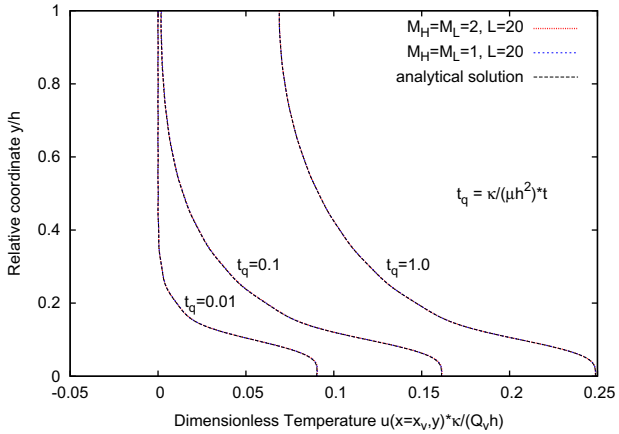

(b) $\frac{\Delta y}{h} = \frac{1}{10}$, 20 modes

Fig. 11. Fully insulated layer, partially subject to uniform unit-step flux. Dimensionless temperature distribution $u(x_v,y)$ at $x = x_v$ and $\bar{t} = 0.01,\ \bar{t} = 0.1,\ \bar{t} = 1.0$.

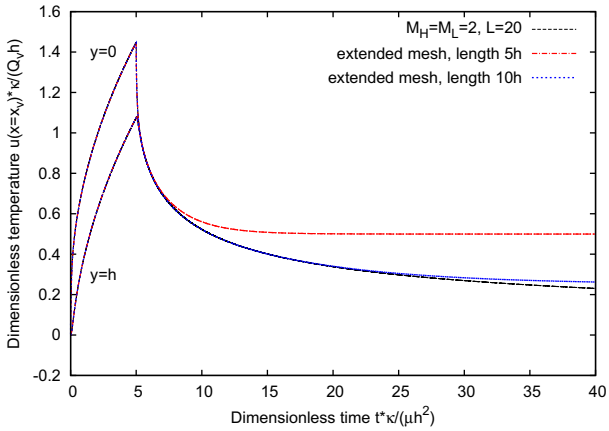

Fig. 12. Fully insulated layer, partially subject to uniform flux for $\bar{t} \leqslant 5.0$ ($\Delta y/h = 0.5$). Dimensionless temperature $u(x_v,t)$ at $x = x_v$ and $y = 0$, $y = h$.

$\bar{t} = 1.0$ obtained using the proposed approach with $M_H = M_L = 2$ or $M_H = M_L = 1$, $L = 20$ is obtained. This confirms the high-accuracy of the method and its correct implementation.

Fig. 12 shows the time-dependence of the computed dimensionless temperature at the top and bottom of the vertical boundary Γ_v due to a prescribed uniform flux $q_v(t)$ acting over half of the width of the layer with:

$$q_v(t) = \begin{cases} Q_v & \text{for } \bar{t} \leqslant 5.0, \\ 0 & \text{for } \bar{t} > 5.0 \end{cases}. \tag{137}$$

The cooling of the layer after a certain period of heating is simulated. It can be seen that a constant distribution of the temperature with respect to the coordinate y is reached shortly after the prescribed heat flux has been released, here approximately $\bar{t} = 5.0$.

To validate the numerical results obtained using the proposed high-order boundary, an extended finite-element mesh is analysed in the time domain. A rectangular region of $h \times 10h$ to the right of the vertical boundary Γ_v is discretized with 4000 four-node elements with the size of $0.05h \times 0.05h$. The response of the bounded rectangular region in an extended mesh is identical to that of the semi-infinite layer at early times, i.e. before a significant part of the region has been heated up, such that a significant error is caused by the fact that the diffusive phenomenon cannot diffuse out. The temperature responses at the surface and at the bottom of the layer obtained from the proposed doubly asymptotic boundary and from the extended mesh method are compared in Fig. 12. Excellent agreement can be observed throughout $\bar{t} < 20.0$. After that, the extended mesh solution approaches a constant value. The solution obtained using the proposed method decays to zero, which corresponds to the correct physical behaviour. An alternative extended mesh solution, which is based on modelling a rectangular region of $h \times 5h$, is also shown in Fig. 12. In this case, the numerical results agree for $\bar{t} < 7.0$, only. This illustrates that the proposed doubly asymptotic open boundary is particularly useful for prolonged diffusion problems, where the use of extended mesh methods becomes inefficient.

Although only step functions have been considered here, the proposed model can be used to simulate the time-dependent distribution of the unknown function $u(x_v,y,t)$ due to arbitrary transient boundary conditions $q_v(t)$.

8. Conclusions

A novel approach to derive a doubly asymptotic high-order open boundary for diffusion in a homogeneous semi-infinite layer has been developed. The proposed formulation is highly accurate throughout the complete Fourier domain. Compared to singly-asymptotic formulations [27,26] a significant gain in accuracy is achieved without additional computational cost. In the examples considered herein, excellent results were obtained using a doubly asymptotic expansion of degree $M_H = M_L = 2$ only. No stability problems occur for higher degrees of approximation.

The continued-fraction open boundary for diffusion in the Fourier domain corresponds to a system of fractional differential equations of order $\alpha = 0.5$ in the time-domain. The computationally disadvantageous non-locality of the fractional operator is eliminated after this system of fractional differential equations is transformed into a local formulation by introducing internal variables. These internal variables are eliminated after time discretization. Thus, the increase in numerical effort due to the use of additional variables is negligible.

Although only diffusion in a semi-infinite layer has been addressed in this paper, the proposed technique is equally applicable to other systems which can be treated by the method of separation of variables, such as the circular cavity or the spherical cavity. More general homogeneous problems can thus be treated by introducing straight, circular or spherical boundaries. Further work related to extending the proposed technique to more general geometries and inhomogeneous problems is in progress. Half-space or full-space problems, where the artificial boundary has corners, can be modelled using the scaled boundary finite element method. The doubly asymptotic solution of the matrix-valued scaled boundary finite-element equation in impedance is the subject of current research.

Acknowledgements

Carolin Birk performed some of the research reported herein during her visit to The University of New South Wales within the scope of a Marie Curie International Outgoing Fellowship for Career Development of the European Union. The financial support provided by the European Union and her appointment as a Visiting Fellow in the School of Civil and Environmental Engineering, The University of New South Wales, are gratefully acknowledged.

References

[1] R.P. Shaw, An integral equation approach to diffusion, International Journal of Heat and Mass Transfer 17 (1974) 693–699.
[2] L.C. Wrobel, C.A. Brebbia, A formulation of the boundary element method for axisymmetric transient heat conduction, International Journal of Heat and Mass Transfer 24 (5) (1981) 843–850.
[3] G.F. Dargush, P.K. Banerjee, Application of the boundary element method to transient heat conduction, International Journal for Numerical Methods in Engineering 31 (1991) 1231–1247.
[4] F.J. Rizzo, D.J. Shippy, A method of solution for certain problems of transient heat conduction, AIAA Journal 8 (1970) 2004–2009.
[5] L.C. Wrobel, C.A. Brebbia, The dual reciprocity boundary element formulation for nonlinear diffusion problems, Computer Methods in Applied Mechanics and Engineering 65 (1987) 147–164.
[6] S.P. Zhu, P. Satravaha, X. Lu, Solving linear diffusion equations with the dual reciprocity method in Laplace space, Engineering Analysis with Boundary Elements 13 (1994) 1–10.

[7] A. Tadeu, J. António, L. Godinho, N. Simões, Boundary element method analyses of transient heat conduction in an unbounded solid layer containing inclusions, Computational Mechanics 34 (2004) 99–110.
[8] D. Givoli, Finite element analysis of heat problems in unbounded domains, in: R.W. Lewis, K. Morgen (Eds.), Numerical Methods in Thermal Problems, vol. VI, Pineridge Press, Swansea, UK, 1989, pp. 1094–1104.
[9] H. Han, Z. Huang, A class of artificial boundary conditions for heat equation in unbounded domains, Computers and Mathematics with Applications 43 (2002) 889–900.
[10] L. Halpern, J. Rauch, Absorbing boundary conditions for diffusion equations, Numerische Mathematik 71 (1995) 185–224.
[11] E. Dubach, Artificial boundary conditions for diffusion equations: numerical study, Journal of Computational and Applied Mathematics 70 (1996) 127–144.
[12] H. Han, Z. Huang, Exact and approximating boundary conditions for the parabolic problems on unbounded domains, Computers and Mathematics with Applications 44 (2002) 655–666.
[13] X. Wu, Z.-Z. Sun, Convergence of difference schemes for heat equation in unbounded domains using artificial boundary conditions, Applied Numerical Mathematics 50 (2004) 261–277.
[14] Z.-Z. Sun, The stability and convergence of an explicit difference scheme for the Schrödinger equation on an infinite domain by using artificial boundary conditions, Journal of Computational Physics 219 (2006) 879–898.
[15] J.-R. Li, L. Greengard, On the numerical solution of the heat equation I: fast solvers in free space, Journal of Computational Physics 226 (2007) 1891–1901.
[16] J. Tausch, A fast method for solving the heat equation by layer potentials, Journal of Computational Physics 224 (2007) 956–969.
[17] X. Antoine, A. Arnold, C. Besse, M. Ehrhardt, A. Schädle, A review of transparent and artificial boundary conditions techniques for linear and nonlinear Schrödinger equations, Communications in Computational Physics 4 (4) (2008) 729–796.
[18] S.V. Tsynkov, Numerical solution of problems on unbounded domains. A review, Applied Numerical Mathematics 27 (1998) 465–532.
[19] D. Givoli, Numerical Methods for Problems in Infinite Domains, Elsevier, 1992.
[20] X. Antoine, C. Besse, Unconditionally stable discretization schemes of non-reflecting boundary conditions for the one-dimensional Schrödinger equation, Journal of Computational Physics 118 (2003) 157–175.
[21] Z. Xu, H. Han, X. Wu, Adaptive absorbing boundary conditions for Schrödinger-type equations: application to nonlinear and multi-dimensional problems, Journal of Computational Physics 225 (2007) 1577–1589.
[22] M. Ehrhardt, C. Zheng, Exact artificial boundary conditions for problems with periodic structures, Journal of Computational Physics 227 (2008) 6877–6894.
[23] T.M. Hagstrom, Asymptotic expansions and boundary conditions for time-dependent problems, SIAM Journal on Numerical Analysis 23 (1986) 948–958.
[24] T.M. Hagstrom, Boundary conditions at outflow for a problem with transport and diffusion, Journal of Computational Physics 69 (1987) 69–80.
[25] A.E. Ioanni, E. Kausel, Heat diffusion in layered media via the thin-layer method, International Journal for Numerical Methods in Engineering 78 (2009) 692–712.
[26] C. Birk, C. Song, A continued-fraction approach for transient diffusion in unbounded medium, Computer Methods in Applied Mechanics and Engineering 198 (2009) 2576–2590.
[27] M.H. Bazyar, C. Song, A continued-fraction based high-order transmitting boundary for wave propagation in unbounded domains of arbitrary geometry, International Journal for Numerical Methods in Engineering 74 (2008) 209–237.
[28] S. Prempramote, C. Song, F. Tin-Loi, G. Lin, High-order doubly asymptotic open boundaries for scalar wave equation, International Journal for Numerical Methods in Engineering 79 (2009) 340–374.
[29] T.L. Geers, Doubly asymptotic approximations for transient motions of submerged structures, Journal of the Acoustical Society of America 63 (1978) 1500–1508.
[30] P. Underwood, T.L. Geers, Doubly asymptotic boundary-element analysis of dynamic soil-structure interaction, International Journal of Solids and Structures 17 (1981) 687–697.
[31] T.L. Geers, B.A. Lewis, Doubly asymptotic approximations for transient elastodynamics, International Journal of Solids and Structures 34 (1997) 1293–1305.
[32] T.L. Geers, Singly and doubly asymptotic computational boundaries, in: T.L. Geers (Ed.), Proceedings of the IUTAM Symposium on Computational Methods for Unbounded Domains, Kluwer Academic Publishers, 1998, pp. 135–141.
[33] T.L. Geers, B.J. Toothaker, Third-order doubly asymptotic approximations for computational acoustics, Journal of Computational Acoustics 8 (2000) 101–120.
[34] F.A. Milinazzo, C.A. Zala, G.H. Brooke, Rational square-root approximations for parabolic equation algorithms, Journal of the Acoustical Society of America 101 (2) (1997) 760–766.
[35] R. Kechroud, X. Antoine, A. Soulaïmani, Numerical accuracy of Padé-type non-reflecting boundary condition for the finite element solution of acoustic scattering problems at high-frequency, International Journal for Numerical Methods in Engineering 64 (2005) 1275–1302.
[36] C. Trinks, P. Ruge, Treatment of dynamic systems with fractional derivatives without evaluating memory–integrals, Computational Mechanics 29 (2002) 471–476.
[37] A.H. Barnett, A fast numerical method for time-resolved photon diffusion in general stratified turbid media, Journal of Computational Physics 201 (2004) 771–797.
[38] M.N. Özisik, Heat Conduction, second ed., John Wiley and Sons, Inc., New York, USA, 1993.
[39] L. Debnath, D. Bhatta, Integral Transforms and Their Applications, second ed., Chapman and Hall/CRC, Boca Raton, FL, 2007.
[40] J.P. Wolf, Consistent lumped–parameter models for unbounded soil: physical representation, Earthquake Engineering and Structural Dynamics 20 (1991) 11–32.
[41] J.P. Wolf, Consistent lumped–parameter models for unbounded soil: frequency–independent stiffness, damping and mass matrices, Earthquake Engineering and Structural Dynamics 20 (1991) 33–41.
[42] I. Podlubny, Fractional differential equations, Mathematics in Science and Engineering, vol. 198, Academic Press Inc., San Diego, California, USA, 1999.
[43] K.B. Oldham, J. Spanier, The fractional calculus, Mathematics in Science and Engineering, vol. 111, Academic Press Inc., San Diego, Boston, New York, London, Sydney, Tokyo, Toronto, 1974.
[44] C.G. Koh, J.M. Kelly, Application of fractional derivatives to seismic analysis of base–isolated models, Earthquake Engineering and Structural Dynamics 19 (1990) 229–241.
[45] W. Zhang, N. Shimizu, Numerical algorithm for dynamic problems involving fractional operators, JSME International Journal Series C 41 (3) (1998) 364–370.
[46] A. Shokooh, L. Suarez, A comparison of numerical methods applied to a fractional model of damping materials, Journal of Vibration and Control 5 (1999) 331–354.
[47] P. Ruge, N. Wagner, Time-domain solutions for vibration systems with fading memory, in: W. Wunderlich (Ed.), European Conference on Computational Mechanics, Munich, Germany, 1999, pp. 367–374 (Published on CD-ROM).
[48] L. Yuan, O.P. Agrawal, A numerical scheme for dynamic systems containing fractional derivatives, Journal of Vibration and Acoustics 124 (2002) 321–324.
[49] S. Jiang, L. Greengard, Fast evaluation of nonreflecting boundary conditions for the Schrödinger equation in one dimension, Computers and Mathematics with Applications 47 (2004) 955–966.
[50] P. Ruge, C. Trinks, Consistent modelling of infinite beams by fractional dynamics, Nonlinear Dynamics 38 (2004) 267–284.

[51] A. Schmidt, L. Gaul, On a critique of a numerical scheme for the calculation of fractionally damped dynamical systems, Mechanics Research Communications 33 (2006) 99–107.
[52] J.-F. Lu, A. Hanyga, Wave field simulation for heterogeneous porous media with singular memory drag force, Journal of Computational Physics 208 (2005) 651–674.
[53] K. Diethelm, An investigation of some nonclassical methods for the numerical approximation of Caputo-type fractional derivatives, Numerical Algorithms 47 (2008) 361–390.
[54] S. Adhikari, N. Wagner, Direct time-domain integration method for exponentially damped linear system, Computers and Structures 82 (2004) 2453–2461.
[55] C. Trinks, Consistent Absorbing Boundaries for Time-domain Interaction Analyses Using the Fractional Calculus, Ph.D. Thesis, Technische Universität Dresden, Fakultät Bauingenieurwesen, 2004.